

AD-A070 756

LAMONT-DOHERTY GEOLOGICAL OBSERVATORY PALISADES N Y

F/G 8/10

TECTONICS OF THE OCEANOGRAPHER TRANSFORM: SEISMIC EVIDENCE, (U)

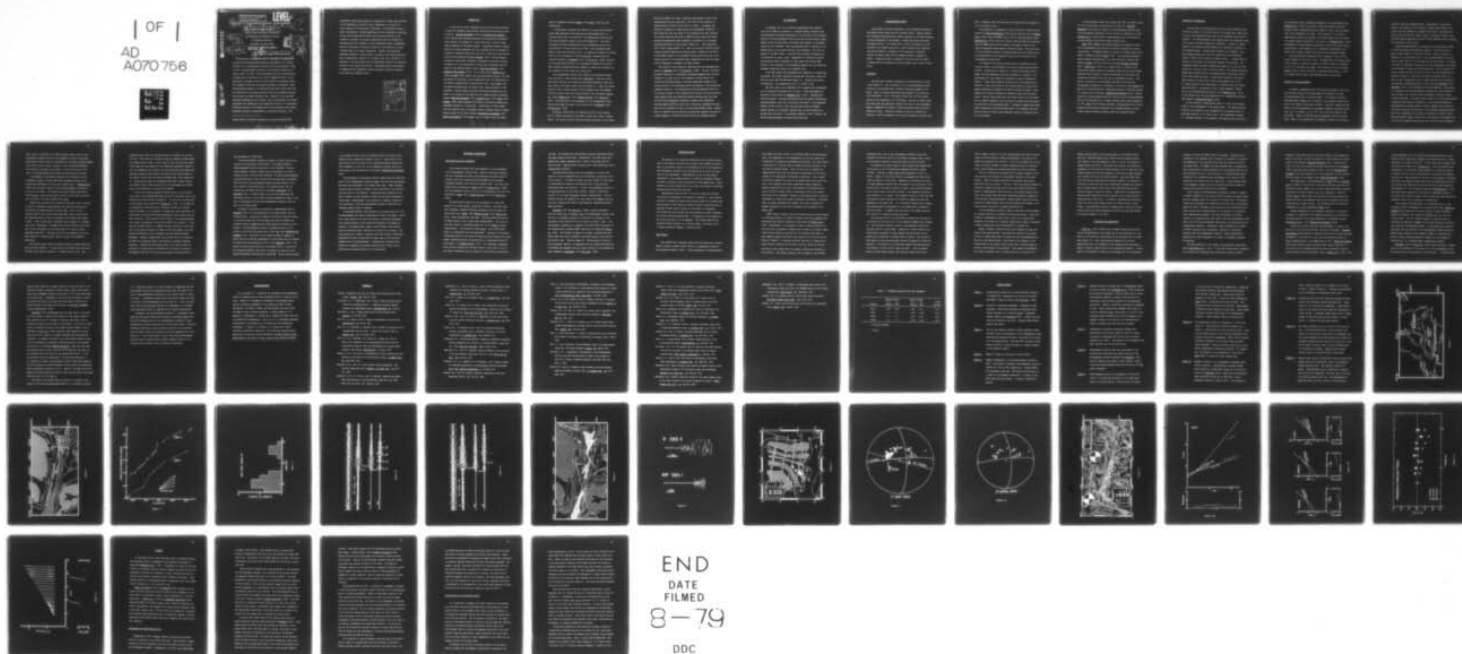
SEP 78 H ROWLETT, O PEREZ

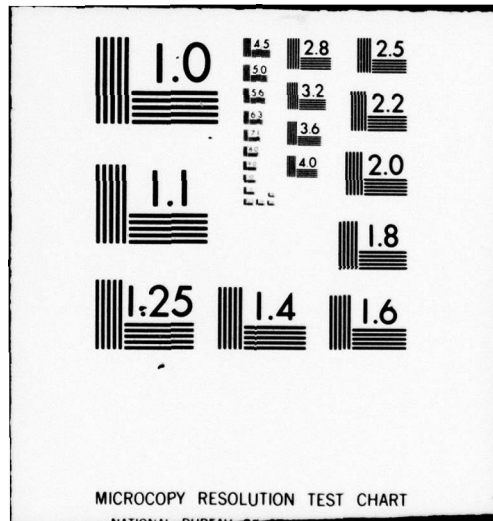
N00014-76-C-0818

UNCLASSIFIED

NL

1 OF 1  
AD  
A070 756





This document has been approved  
for public release and sale; its  
distribution is unlimited.

# LEVEL II

## TECTONICS OF THE OCEANOGRAPHER TRANSFORM: SEISMIC EVIDENCE<sup>1</sup>

10 Hugh/Rowlett and Omar/Perez

Lamont-Doherty Geological Observatory

and Department of Geological Sciences

of Columbia University

Palisades, New York 10964

Contract No. N00014-76-C-0818<sup>12</sup>  
Date: Sept. 1978

### ABSTRACT

15 N00014-76-C-0818, NSF-DES74-24698

11 Sep 78  
12 68 p  
136 130

→ Ocean-bottom seismographs (OBS's) were used in a combined re-  
fraction and microearthquake monitoring experiment at the eastern  
junction of the Oceanographer transform with the mid-Atlantic ridge  
at 35°N. Microearthquake activity at the junction occurred over a  
zone at least 7 km wide. Microearthquakes that were located define  
a linear zone of faulting up to 12 km in length and about 3 km in  
width that is oblique to both the local strike of the median valley  
and transform valley and the present direction of spreading. These  
microearthquakes appear to be associated with fault scarps that form  
the inner walls on the west and north sides of the median and trans-  
form valleys. A simple transform fault, parallel to the east-west  
spreading direction at this latitude, was not delineated by the micro-  
earthquakes even though the focal-mechanism solution of a teleseismic  
earthquake located at the western end of the transform clearly shows  
transform faulting in approximately an east-west direction. The

<sup>1</sup>Lamont-Doherty Geological Observatory Contribution Number 0000.

79 06 19 006 (3)

teleseismic observations support the suggestion of others that portions of the transform are currently under compression as a result of a recent change in the direction of spreading. The limited microearthquake observations, although suggesting that the transition of faulting between the northern median valley and the eastern portion of the transform is gradual and probably complicated, does not confirm the hypothesis that the transform is under compression since a complicated pattern of faulting is observed by others at the junction of a large transform that is not under compression. Finally, the refraction experiment defined a 3 km/sec layer, 1 km thick, that overlies material with a compressional velocity of 5.6 km/sec near one of the OBS's. A prominent, 8 km long, shadow zone for ground-wave arrivals was observed from one of the refraction profiles. This shadow zone is interpreted as suggesting that significant lateral changes in velocity structure occur along the transform valley.

Accession For	
NTIS GMA&I	<input checked="" type="checkbox"/>
DDC TAB	<input type="checkbox"/>
Unannounced	<input type="checkbox"/>
Justification <i>for the</i>	<input type="checkbox"/>
<i>on file</i>	
By	
Distribution/	
Availability Codes	
Dist	Avail and/or special
<i>A</i>	



### INTRODUCTION

In the last few years techniques and data have become available to study the seismicity and tectonics associated with fracture zones in detail. Reid and Macdonald [1973] and Macdonald and Luyendyk [1977] observe that faulting associated with present-day microearthquake activity is confined to a narrow zone about 1 km wide along small transforms of the North Atlantic. Submersible studies, however, show for the same transforms that the transform valley is defined by a series of parallel faults that occur over a wider zone than the presently active transform faulting [Arcyana, 1975]. Microearthquake activity in these small transforms, presumably strike-slip faulting, continues up to the intersection of these small transforms with the center of the adjacent median valleys [Reid and Macdonald, 1973; Macdonald and Luyendyk, 1977]. On the other hand, Prothero et al. [1976] and Reid [1976] observe that microearthquake activity, and thus the pattern of faulting, is more complicated near the intersection of the Rivera transform with the East Pacific Rise. They suggest that an echelon faulting occurs on several fault planes parallel to this transform. Several studies also show that microearthquakes are confined to the portion of the fracture zone between adjacent spreading centers [Reid and Macdonald, 1973; Prothero et al., 1976; Reid, 1976; Francis, 1976], which supports the theory of sea-floor spreading and transform faulting on a local-scale. Observations of fault scarps that both parallel and cut obliquely across transform valleys of small fracture zones in the North Atlantic [Whitmarsh and Laughton, 1976; Searle and Laughton, 1977] suggest that on a small scale the simple

79 06 19 006

model of transform faulting [Wilson, 1965; Sykes, 1967] may need modification.

In this paper we present the results of an ocean-bottom seismograph (OBS) experiment that monitored microearthquakes and a refraction survey near the junction of the Oceanographer fracture zone with the mid-Atlantic ridge at 35°N, 35°W (Figure 1). This study represents the first observations of microearthquake activity near the junction of a major fracture zone with a slow spreading system (about 1 cm/yr half spreading rate). We compare the results of the OBS study with the bathymetry of the Oceanographer transform that was recently published by Schroeder [1977] and Fox et al. [1978], and with the focal-mechanism solution of an earthquake recorded by the World-Wide Standard Seismograph Network (WWSSN) to examine the tectonics of the transform on both a small and large scale.

The Oceanographer fracture zone offsets the mid-Atlantic ridge about 128 km in a right lateral sense [Fox et al., 1978] and is the first major fracture zone along the North American/African plate boundary south of the Azores triple junction (Figure 1). Since its initial survey in 1967, several studies of the bathymetry and rocks dredged from the fracture zones have been published in the literature [Fox et al., 1969; Pitman et al., 1974; Shibata and Fox, 1975; Fox et al., 1976]. The discussion of the bathymetry of the Oceanographer transform in this paper are based on the recent work of Schroeder [1977] and Fox et al. [1978].

Fox et al. observe that the transform portion of the fracture zone is clearly delineated by the 3000 m contour and a deep, V-shaped valley. The valley is narrow and well-defined along most of the trans-



form but broadens into large, triangular depressions at both of the intersections with the ridge axis. The floor of the transform is characterized by relief of about 500 m to 1400 m. Fox et al. and Schroeder recognize two trends along the Oceanographer transform: a N74°W direction near the center of the transform that they interpret as an older spreading direction; a N88°E direction near both ridge/transform intersections that presumably is parallel to the present spreading direction at this latitude (Figure 11). They hypothesize that a recent change (about 3 m.y. ago) in the pole of relative motion between the North American and African plates, recorded by the N74°W and the N88°E trends of the transform valley, places the crust of the central portion of the transform under compression and that the transform is deforming to eliminate the ridge overlap.

The results of this study are consistent with the hypothesis presented by Schroeder [1977] and Fox et al. [1978]. In fact, the focal-mechanism solution of a teleseismic earthquake suggests that the main response of at least part of the transform to plate motion is by strike-slip faulting oblique to the main bathymetric trends of the central portion of the transform valley and parallel to the present-day spreading direction. The distribution of microearthquake activity at the eastern junction of the transform with the axis of the mid-Atlantic ridge suggests that the transition between faulting along the ridge axis and the Oceanographer transform is gradual with significant microearthquake activity located over a wide zone, including the walls north of the transform and west of the adjacent median valley. Finally, there is evidence from the refraction survey that supports the idea of lateral changes in velocity structure within the transform valley.

### OBS EXPERIMENT

In November 1974 two ocean-bottom seismographs were deployed from the R/V VEMA as receivers in a combined seismic refraction and microearthquake monitoring experiment at the junction of the transform section of the Oceanographer fracture zone and the mid-Atlantic ridge. Figure 2 shows the positions of the OBS's with respect to the median valley and the transform. OBS 1 was deployed about 12 km west of the median valley in the central valley of the transform. OBS 3 was deployed 9.7 km ENE of OBS 1. Both OBS units recorded continuously on the sea-floor for about 5 days. Examination of reflection profiles and precision depth recordings (3.5 kHz) taken from several VEMA cruises in the vicinity of the deployments suggest that the bottom was extremely rough with little or no sediment cover.

A few hours before the instruments were scheduled to release from the bottom, four short refraction profiles were shot west to east and south to north over the OBS array (Figure 2). Tetrytol was used as the explosive. Two charges were used, 1.4 kg and 2.5 kg.

OBS units used in this experiment were equipped with a hydrophone and two geophones (horizontal and vertical). These instruments are discussed in more detail by McDonald et al. [1977]. Although OBS 1 operated properly, recording refractions from the seismic profiles and microearthquakes, there were difficulties with OBS 3. The hydrophone channel of OBS 3 did not record any data and we did not observe seismic phases on the geophone channels that we could interpret as ground waves from shots. The geophone channels of OBS 3, however, did record microearthquakes and water waves from shots.



### MICROEARTHQUAKE SURVEY

One problem of tectonic importance is how spreading processes at the median valley change near the transform valley. Several workers have addressed this problem near small transforms in the North Atlantic by detailed mapping of the basement, submersible studies and micro-earthquake surveys. Our purpose was to study the seismicity at the junction of the median valley with a major transform fault (greater than 100 km offset) to determine if the transition of faulting between the median valley and the transform valley is gradual or abrupt. Though this study is limited by the use of only two OBS's, it argues that the transition at 35°N is gradual over a scale of about 20 km.

### Seismicity

Both OBS units recorded continuously on the sea-floor for about 5 days (Figure 2). OBS 3 recorded up to 111 microearthquakes during 129 hours on the bottom; OBS 1 recorded 75 microearthquakes in 110 hours. Only 20 of these events were large enough to be recorded by both instruments. Two of the largest events were from the central portion of the transform, 70 to 90 km away. The rest of these events were very small and apparently occurred near each of the instruments. Figure 3 summarizes the number of events recorded by OBS 1 and OBS 3 during the 5 days. (The data in Figure 3 were not corrected for distance.) With the exception of two short increases in activity near

OBS 3, seismicity near both OBS units was similar with an average of 15 to 20 events per day.

The seismicity is comparable to rates of about 10 events per day observed by Reid and Macdonald [1973] and 36 events per day by Spindel et al. [1974] near the FAMOUS area at 37°N on the mid-Atlantic ridge. Francis et al. [1977] point out, however, that the level of seismicity near the FAMOUS area can vary during a few months as much as two orders of magnitude along adjacent transform faults. Thus, the level of activity during the short recording interval of this study may not be representative of the long-term activity of the junction of the Oceanographer fracture zone.

In contrast to the nearly constant level of seismicity in the vicinity of OBS 1, two increases in the rate of events were detected at OBS 3. During day 335 (Figure 3), 33 events with signal levels higher than the background noise were recorded in 12 minutes. The distribution of these events as a function of time is presented in Figure 4. These events probably occurred only a few hundred meters from OBS 3, which was located on the northern edge of a large topographic depression (outlined by the 4200 m contour in Figure 2) that dominates the junction between the transform valley and the median valley. Because these events were very close to OBS 3, it was difficult to identify separate P and S arrivals to confirm that this group of events was a microearthquake swarm. Although we suggest that these events represented a microearthquake swarm, it is possible that they were the result of either small submarine slides or biological noise at the instrument.



A microearthquake swarm that occurred near OBS 3 is shown in Figure 3 by the increase in event activity on day 337. Reid and Macdonald [1973] observe a swarm of microearthquakes along the edge of the bathymetric depression at the west end of transform A at 37°N. Prothero et al. [1976] report a swarm sequence near the junction of the East Pacific Rise with the Rivera fracture zone.

Mogi [1963] suggests that swarm sequences are limited to areas with a heterogeneous distribution of material properties and stress concentration. Earthquake swarms are typical of volcanic areas and of areas of submarine rifting [Sykes, 1970]. The faulting mechanism of swarms observed teleseismically are characterized by either normal faulting [Sykes, 1970] or strike-slip faulting [Tatham and Savino, 1974]. Klein et al. [1977], in a detail study of a swarm in the transitional region between the Reykjanes ridge and the south Iceland transform fault, observed a swarm characterized by both normal and strike-slip faulting in the same zone of earthquake activity. Similarly, the portion of crust between the median valley and the Oceanographer transform may correspond to the type of area suggested by Mogi and be characterized by a complicated pattern of faulting instead of a single type of faulting. Macdonald and Luyendyk [1977], however, observed a microearthquake swarm and a narrow zone of microearthquakes that can be reconciled with a single transform fault along transform A at 37°N. Hill [1977] recently published a working model of the stress orientation and faulting mechanisms for earthquake swarms in transitional regions between spreading centers and transform faults.

### Character of Seismograms

We found that the large amplitude of the S phase recorded on the horizontal channel of both OBS's useful for counting small events that are below the background noise levels on the hydrophone and vertical channels. For microearthquakes with signals above the background noise level several different phases were identified. In Figure 5 seismograms of two different microearthquakes are presented as examples of the observed phases. P phases were recorded on all channels. The best signal-to-noise ratio for the P phase was on the hydrophone channel of OBS 1 and the vertical channel of OBS 3. S phases were recorded on the vertical and horizontal channels of both OBS's. The hydrophone channel recorded compressional phases ( $R_1$ ,  $R_2$  and  $R_3$ ) that reflect up to several times at the sea surface. The surface-reflected phases were recorded only by the hydrophone since this phase arrives at the OBS through the water. T phases were observed on the hydrophone channel for events with S and P times greater than 2.0 sec. At closer distances the T phase begins to interfere with the surface-reflected phases. The presence of the T phase suggests a shallow source for microearthquakes recorded at sea [Francis et al., 1977]. In this paper we use the same nomenclature for identifying microearthquake phases as Francis and Porter [1973].

We also identify a compressional phase,  $P'$ , that occurs between P and S on the seismograms of the larger events. The signal-to-noise ratio was not favorable on the seismograms of the smaller events to positively identify  $P'$  for these events. Both instruments recorded  $P'$ . Although recorded on all channels, this phase was best observed on



the hydrophone channel suggesting propagation as a compressional wave. Francis et al. [1977] also observe, during OBS studies on the mid-Atlantic ridge, compressional phases similar to the P' that we observe here (also designated P' by them). They interpret P' as a direct compressional phase that propagates at shallow depths in the low velocity surface layer [equivalent to the layer 2A of Talwani et al., 1971]. Earthquakes with these phases are probably located in the low-velocity surface layer. This appears to be a reasonable interpretation of P'. They do not, however, observe this phase on the horizontal channel.

The time difference measured on OBS 1 between P' and P, (P'-P), varies between 0.45 sec and 0.73 sec. Although there is scatter in the (P'-P) times as a function of range to the OBS's, there is a tendency for (P'-P) to increase with range. The increase in (P'-P) with range suggests that P' may be refracted at shallower depths than P. It is not possible here to make a more detailed study of this phase.

#### Location of Microearthquakes

In general, assumptions about the velocity structure of the crust and the focal depths of microearthquakes are necessary to locate microearthquakes from a two-station array. The refraction results, discussed later, suggest that 5.6 km/sec is the dominant crustal velocity in the central valley near the OBS's. Therefore, ranges from the OBS's to the microearthquakes are computed assuming a half-space model with a  $V_p = 5.6$  km/sec,  $V_s = V_p / \sqrt{3}$  and a zero focal depth in the half-space. These are obviously gross assumptions, since as we show later, there is the possibility of substantial changes in the velocity

structure along the transform valley. Nevertheless, as mentioned earlier, the presence of the T phase for longer-range events is consistent with the assumption of shallow focal depth. Epicenters calculated from the data set, using a range of reasonable values for  $V_p$  and focal depths, generally move only a few kilometers without changing the conclusions of this study.

Seven microearthquakes are located this way using phases picked on both the geophone and hydrophone channels. These events have S minus P times between 1.10 sec and 2.83 sec. There is, however, an ambiguity in the locations; that is, the microearthquakes can be located on either side of a line through the two OBS stations. In Figure 6 we show the epicentral locations of the microearthquakes with respect to the basement contours and the OBS positions. The two possible locations (closed and open circles) for each of the microearthquakes are plotted in Figure 6. Even with the limited recording interval of 5 days, it may be significant that a simple transform fault parallel to the east-west spreading direction at this latitude [Macdonald, 1977; Schroeder, 1977] is not delineated by microearthquakes. Nevertheless, it is possible that microearthquakes occurring near the instruments, and too small to be located by both instruments, represent simple transform faulting. The linear trend of either zone of microearthquakes (closed and open circles) in Figure 6, if the microearthquakes are associated with the same system of faults, suggests that faulting at the junction may not occur parallel to the present spreading direction. Note that, regardless of the choice of epicentral location for each microearthquake, seismic activity near the junction of the median valley with the transform valley occurs over an area several kilometers



wide, since, in addition to the seven located events, there is also considerable seismic activity in the immediate vicinity of each OBS. When seismic activity near the instruments is included, microearthquakes occur over an area at least 7 km wide, if all the microearthquakes were located on one side of the array, or over an area up to 14 km wide, if microearthquakes were located on both sides of the array.

The ambiguity in epicentral locations can be resolved, if the bathymetry is known, from the additional information given by the travel-time differences of the  $R_1$  and P phases ( $R_1$ -P). Francis et al. [1977] also use ( $R_1$ -P) times to locate microearthquakes recorded by an array of two OBS's. The method we use here differs from that of Francis et al., since we have better control on the crustal structure near the sites of our OBS's than Francis et al.

Because the ray-path for  $R_1$  crosses the sea-floor about 2 km from an OBS (for reasonable crustal models), the velocity structure near the OBS has the greater effect on ( $R_1$ -P) times. Thus, we use a velocity model of the central valley near OBS 1 that we derive from the refraction data to test for locations of the events with respect to OBS 1. This crustal model, discussed later, consists of a dipping layer over a half-space. We assume that the main refractor (the boundary of the half-space) of the crustal model is a plane in three-dimensions near OBS 1. This way we can vary the apparent dip of the main refractor to compute ( $R_1$ -P) times for events from different directions.

We calculate ( $R_1$ -P) times for sources located at depths above and below the main refractor. In cases where the refractor dips away from the OBS, ( $R_1$ -P) times are equal to or greater than 5.13 sec. The

observed ( $R_1$ -P) times for the seven events are between 4.91 sec and 5.05 sec. Only cases with refractors that dip towards the OBS satisfy the observed ( $R_1$ -P) times. Travel times of first arrivals from shots fired along the south profile of the refraction experiment (Figure 2) over the transform valley require (if the refractions from these shots propagate along the same refractor derived for the velocity model of the central valley) that the refractor beneath OBS 1 dips towards the SE. These results imply that epicenters SE of OBS 1 cannot satisfy the observed ( $R_1$ -P) times and that all of the epicenters are located north of the OBS array in a zone that trends NE.

If all of the seven epicenters occurred south of the two OBS's, they define a zone trending WNW along the base of the south wall of the fracture zone (open circles in Figure 6). In this area the south wall of the fracture zone trends N74°W [Fox et al., 1978]. If the WNW zone of epicenters is associated with a system of faults with the same type of faulting, it is reasonable to assume that these epicenters had left-lateral, strike-slip faulting mechanisms on fault planes that are nearly vertical. First motions from all seven of the microearthquakes were clearly dilatational at both of the OBS's (e.g., Figure 7). Even with the possible effect of a complex velocity structure on the variation of the take-off angles of P waves at the focal sphere, the first motion observations are not consistent with the assumed faulting mechanism. Instead, compressional first motions would be recorded by the OBS's for epicenters with a left-lateral, strike-slip faulting mechanism. Although the first-motion data do not favor a choice of epicentral locations south of the OBS's for all seven of the microearthquakes, the data do not preclude epicentral locations south of



the instruments on a WNW trend.

The microearthquake locations in Figure 6 (closed circles) are located in an area where the west wall of the median valley is indistinguishable from the north wall of the transform. The epicenters appear to define a linear zone of faulting up to 12 km in length and about 3 km wide that trends NE. If these microearthquakes are associated with a zone of faults with the same type of faulting, then the trend of the earthquakes suggest faulting oblique to the local strike of the median valley, the transform valley and the present-day, east-west direction of spreading [Macdonald, 1977; Schroeder, 1977]. Locating these events with any reasonable compressional velocity or focal depth although changing the angle of the zone of earthquakes with the main physiographic features, still results in an oblique trend.

In Figure 8 epicenters are plotted on a physiographic map by Schroeder [1977] of the intersection of the median valley with the transform fault. Epicenters in Figure 8 are located along the trends of the major scarps that form the inner wall above the median and transform valleys, suggesting that these scarps are presently active features. Microearthquakes located in the median valley at 37°N cluster at the first and second steps of the inner wall [Macdonald and Luyendyk, 1977]. The relief of the scarps in Figure 8 appears to result from the step-like arrangement of tilted blocks that dip towards the inner floor with gradients of 10° to 40° [Schroeder, 1977]. The strike of scarps along the walls of the median valley on the side of the transform gradually bend around, following the contours as the transform-spreading intersection is approached. Scarps along the walls

on the opposite (east) side of the median valley do not bend as the fracture zone is approached (Figures 6 and 8). Small faults in the inner floor of the rift axis at the transform-spreading intersection with transform A at 37°N cut across bathymetric contours and do not bend around as the intersection is approached [Macdonald and Luyendyk, 1977].

The association of epicenters with the scarps along the inner wall north of the Oceanographer transform suggest that the microearthquakes may have focal mechanisms of the normal fault type. Normal faulting along the oblique scarps in Figure 8 could contribute to the relief of the north wall of the transform. First-motion data observed at the OBS's, however, are not adequate to solve for the focal mechanisms of these events. Nevertheless, first motions of P arrivals, because of the distribution of the microearthquakes relative to the OBS's, can eliminate several types of faulting.

As mentioned earlier, first motions of P arrivals from all of the microearthquakes are clearly dilatational at both of the OBS's. Therefore, these events do not have left-lateral, strike-slip mechanisms with strikes parallel to the present-day direction of spreading or parallel to the mapped fault scarps, since different first motions would be detected at OBS 1 and OBS 3 for several of the events. The first motions are, however, consistent with left-lateral, strike-slip mechanisms that have strikes with the same trend as the entire NE-trending zone of microearthquakes. Alternatively, observed first motions are consistent with normal faulting of any strike if the P waves leave the bottom portion of the focal-sphere.



## TELESEISMIC OBSERVATIONS

### Earthquakes Along the Transform

Fault-plane solutions have been examined for two earthquakes on the Oceanographer fracture zone. These two solutions represent the only earthquakes for which focal-mechanism solutions could be studied, using only body-wave data from WWSSN and the Canadian Seismograph Network, from 1962 until December 1976. The basic techniques used are discussed by Sykes [1967] and Isacks et al. [1969]. The focal-mechanism solution of one of the earthquakes, May 1974, was published by Sykes [1967], Weidner and Aki [1973] and Udias et al. [1976].

The fault-plane solution for the earthquake of 17 May 1964 (event 1) is a left-lateral, strike-slip solution. The nodal plane that represents transform faulting, determined from both body and surface wave data [Sykes, 1967; Weidner and Aki, 1973; Udias et al., 1976], trends approximately east-west. The focal-mechanism solution of Sykes (Figure 9) has a nodal plane trending N86°E. The strike of this nodal plane is constrained within 15° to 20° [Sykes, personal communication]. The solution of Udias et al., with a N90°E nodal plane, is constrained about the same amount. Analysis of the spectra of Rayleigh waves for this event by Weidner and Aki indicate that nodal planes trending east-west and north-south are constrained within 10° [see Figure 9 of Weidner and Aki, 1973]. We re-examined seismograms from stations located near the nodal planes of this event to see if any better constraints could be placed on the fault-plane solution by

the data. We conclude that the published solutions accurately define the nodal planes of this event. Specifically, the nodal plane that defines the present transform fault, cannot be more than about  $8^{\circ}$  north of west. (SHA and other stations north of SHA definitely record compressional arrivals.)

The fault-plane solution for the earthquake of 17 April 1974 (event 3) is also consistent with the left-lateral, strike-slip solution of event 1. As Figure 10 shows, the nodal planes for this event is constrained too poorly by the body-wave data to make specific conclusions about the tectonics. A study of the amplitude spectra of the Rayleigh waves of this event, however, confirm a strike-slip solution for the event [S. K. Ho, personal communication]. The preliminary surface wave analysis for that event by Ho suggests that the east-west trending nodal plane is approximately constrained between  $N80^{\circ}E$  and  $N84^{\circ}E$ .

Schroeder [1977] and Fox et al. [1978], recently published a detailed contour map of basement along the Oceanographer fracture zone. This map is presented in Figure 11 along with the solution of the earthquake of May 1964 and the ISC locations of events 1 and 3. The Oceanographer transform is a composite of a  $N74^{\circ}W$  trend along most of the transform and a possible  $N88^{\circ}W$  trend near the ridge axes [Fox et al., 1978]. The solution in Figure 11 of event 1 (strike-slip mechanism) shows that slip is oblique to the  $N74^{\circ}W$  trend of the center of the fracture zone. (See also Figure 9.) The direction of slip for this earthquake, however, is compatible with the present-day direction of spreading and suggests that the central portion of the transform is under compression [Schroeder, 1977; Fox et al., 1978].



### REFRACTION SURVEY

The purpose of the refraction experiment was to provide an estimate of the velocity structure of the upper crust beneath the instruments in the central valley of the transform to aid in the location of microearthquakes recorded by the instruments and to locate the positions of the instruments. Unfortunately, we did not have enough instruments or long enough profiles to obtain the information needed to derive a detailed velocity structure for this complex area. Nevertheless, even this limited data set was useful and several interesting observations are made from this data.

Time-distance plots for OBS 1 of the four refraction profiles (corrected for topography) are presented in Figure 12. Least-squares solutions for apparent velocity and intercept times of the travel-time lines plotted in this figure are listed in Table 1 along with the coefficient ( $dt/dh$ ) used to correct for the effect of topography.

Travel-time data from the east and west profiles are used to estimate the crustal structure beneath OBS 1. A discussion of the analysis of the travel-time data is in the Appendix. The crustal model of the transform valley consists of a 3.0 km/sec layer, 1 km thick, over a 5.6 km/sec refractor dipping  $2^\circ$  towards the east.

#### West Profile

This profile has a prominent shadow zone for ground wave arrivals. Figure 14 shows a reduced record section of seismograms recorded on the hydrophone channel of OBS 1. These seismograms are hand-digitized

from before the first arrival to the arrival time of the direct water wave. The amplitudes of the seismograms on the record section are uncorrected for geometrical spreading and shot size. For this profile a shot size of 1.4 kg was used for ranges less than 8 km and 2.5 kg was used for greater ranges. Since the shot size is constant for ranges greater than 8 km, the variation in amplitudes on the record section is not explained by variations in shot size. Thus, crustal structure is probably the cause of the shadow zone on the record section. This suggests that either significant lateral changes in seismic properties occur in the crust beneath the shooting track or that a velocity reversal occurs at some depth in the crust beneath the valley of the transform. Because we have observations at only one instrument, we cannot prove either hypothesis conclusively. Nevertheless, we present arguments that suggest that lateral variation in seismic properties of the crust can explain the occurrence of the shadow zone.

Shadow zones as large as the one we observe have not been detected by refraction surveys over areas of oceanic crust that presumably are associated with velocity reversals in the crust [see Orcutt et al., 1976]. Nevertheless, it is possible to have a velocity structure in the crust that can generate a shadow zone as large as we observe (about 8 km) if the velocity at the base of a low velocity zone (LVZ) is only slightly greater than that of the velocity of the lid of the LVZ (about 0.1 km/sec). A velocity structure like this, if there are no sharp velocity contrasts at the base of the LVZ, would also explain the lack of other energy from, for example, reflections returning to the sea-floor. One feature, however, that is common to all velocity



structures with a LVZ is that the apparent velocity of rays that penetrate the LVZ and return to the surface is greater than or equal to the apparent velocity of rays that graze the top of the LVZ.

We measured the travel times of first arrivals with ranges from 18.8 km and 21.5 km to calculate the apparent velocity of these arrivals. Arrivals at these ranges should penetrate a LVZ if it exists. Several of the first arrivals are emergent and their travel times are subject to some error. Therefore, we correlate the phases of larger amplitude arrivals that correspond to the oscillation of the bubble pulse of the first arrivals to obtain a more accurate estimate of the arrival time of the first arrivals. The apparent velocity of these arrivals is 5.1 km/sec. This apparent velocity is less than that calculated for first arrivals (5.9 km/sec) at ranges less than the beginning of the shadow zone. It is therefore unlikely that a simple, flat-layered model is responsible for the shadow zone we observe on the west profile. It appears that the cause of the shadow zone may be a result of a laterally varying structure.

The shooting track of the west profile crosses over the base of a protrusion on the north wall of the transform (dashed line in Figure 2). This protrusion displays itself in the bathymetry beneath the shooting track as a large ridge. Inspection of return echoes on precision depth recordings (3.5 kHz) suggest that the surface of the protrusion is rough and is probably heavily faulted. The outline of this feature on the precision depth records is defined by a series of hyperbola. The portion of the protrusion beneath the shooting track lies between 7 km and 18 km in range from OBS 1. This is approximately the same range interval over which the shadow zone occurs.



This is shown in Figure 15 by the locations where rays (near vertical lines) from shots fired at ranges corresponding to the edge of the shadow zone penetrate the sea-floor. Thus, if the shadow zone is the result of lateral changes in seismic properties along the shooting track, these changes are probably associated with this protrusion.

We try to determine in a general way if lateral changes in velocity structure can account for the general features of the record section. There are several features of the record section that a model must take into account. They are: first and second arrivals are observed at ranges less than 10 km; first and second arrivals disappear at ranges greater than 10 km over a very short distance (less than 1 km); ground waves with small amplitudes gradually reappear at 15 km and have larger amplitudes at ranges greater than 18 km; first arrivals at ranges greater than 18 km are delayed with respect to the first arrivals that occur at ranges less than 10 km.

In the following we present a model to show that lateral changes in velocity structure can explain the above observations. Since this profile is unreversed we cannot hope to solve for a unique model. Therefore, this model is by necessity simple and is meant to represent a class of models that can be interpreted in a general way.

Figure 15 shows a structure section that explains the main features of the record section. This model was tested by ray tracing to see if a shadow zone could be created with the same dimensions as the one on the record section. This model is very similar to the crustal model of the central valley except that a lateral change in velocity occurs beneath the protrusion. This change is represented by a block of material that is thicker than the low velocity (3.0

km/sec) surface layer of the velocity model of the central valley, that has a velocity greater than 4 km/sec and that produces travel time delays of the right magnitude (0.28 to 0.5 sec) for arrivals at ranges greater than 18 km. This model also produces the abrupt disappearance of both first and second arrivals at 10 km, since rays from greater ranges will cross the boundary of the block at angles greater than critical for first and second arrivals. Rays from shots fired over the block are reflected from the main refractor (5.6 km/sec) of the central valley into the water column before reaching the receiver. Only at ranges greater than 15 km do rays reflected from the main refractor begin to reach the receiver. These rays are interpreted as producing small amplitude arrivals observed on the record section at ranges between 15 and 18 km. In practice, scattering and refraction within the block could instead produce the weak arrivals at these ranges. Large amplitude arrivals at ranges greater than 18 km on the record section are easily explained by refractions that pass through the western boundary of the block.

#### DISCUSSION AND CONCLUSIONS

Fox et al. [1978] consider that the N88°E trend accurately describes the morphology of the younger wall of the transform for a distance of 25 km near the intersections of the transform with the ridge axis (Figure 11). Their interpretation appears to be an oversimplification since the bathymetry of the transform near the ridge on Figure 11 shows no single trend for any appreciable distance. In fact, many of the bathymetric contours on the younger wall of the transform



actually cut across the N88°E trend of Fox et al. Considering the resolution of the basement shown in Figure 11, we prefer to interpret the morphology of the transform valley near the ridge axis without any single trend. We suggest the plate boundary here is complicated. This interpretation is more consistent with the observed wide zone of microearthquake activity, the occurrence of a microearthquake swarm, widening of the transform valley and bending of the traces of fault scarps near the junction with the ridge axis. A more detailed study of the basement, however, may show localized structural trends that parallel the present-day direction of spreading.

Fault scarps and microearthquake epicenters in Figure 8 suggest a gradual transition of the strike of faults between the median valley and the transform valley on the scale of at least 20 km. The gradual transition of faulting, also exhibited by the wide zone of microearthquakes (at least 7 km wide) at the junction of the transform with the median valley, may be characteristic of the junction of a transform under compressional stresses. Two other transforms in the North Atlantic, one larger and the other smaller than the Oceanographer transform, have active plate boundaries that appear to be narrower than the Oceanographer transform. Furthermore, these transforms also exhibit a sharper transition from accretionary tectonics to strike-slip tectonics than the Oceanographer transform. These transforms are apparently not under compression as a result of changing directions of spreading.

The Vema transform at 11°N offsets the mid-Atlantic ridge about 300 km [Van Andel et al., 1971]. At the Vema fracture zone, accretionary tectonics are transformed into strike-slip tectonics within a



distance of less than 10 km and the active trace of the transform is narrow, less than 2 km wide, as shown by 3.5 kHz traverses over sediments in the transform [Eittreim and Ewing, 1975]. Along fracture zone A at 37°N, which offsets the median valley about 20 km [Arcyana, 1975], the active plate boundary is about 1 km wide [Macdonald and Luyendyk, 1977] and continues up to the intersection of the transform with the center of the median valley [Reid and Macdonald, 1973].

The observations of microearthquakes by Reid [1976] and Prothero et al., [1976] for the junction of the Rivera fracture zone with the East Pacific Rise, suggest that the above comparison between transform junctions in the North Atlantic may be too simplistic. Reid and Prothero et al. observe that the transition of faulting between the western portion of the transform with the rise is gradual and occurs along several en echelon faults. The western portion of the Rivera transform is not under compression [Reid, 1976].

Another explanation of the seismicity observed at the junction is based on a comparison of the observed faulting at the junction to faulting observed in clay model experiments of transform faulting [Courtillot et al., 1974; Whitmarsh and Laughton, 1976].

Trends of the fault scarps and microearthquakes in Figure 8 are about 30° to 50° from the east-west direction of spreading. Whitmarsh and Laughton [1976] observe on side-scan sonar mosaics oblique faulting trending 15° to 35° and 30° to 60° from the spreading direction on small transform faults in the FAMOUS area at 37°N. Searle and Laughton [1977] also observe on their side-scan sonar mosaics faulting 8° to 38° oblique to the spreading direction along the Kurchatov fracture zone at 40°30'N on the mid-Atlantic ridge. Francis et al. [1977], from

an OBS experiment near 37°N, observe microearthquakes with a linear pattern 6 km in length that intersects the eastern portion of a small transform at an angle of about 31°. All of these studies suggest that the wrench fault model [e.g., Wilcox et al., 1973] may explain their observations. In this model "Riedel shears" are typically oriented at angles of 20° or less to the direction of pure shear and tensional faulting is at angles between 30° and 60° to the direction of shearing. This model also predicts normal faults near the intersection with the rift valleys that bend away from the rift valley and reach angles of approximately 45° to the spreading direction [Cortillot et al., 1974]. The normal faults predicted by the model are remarkably similar to the active fault scarps in Figure 8 with strikes that bend towards the transform valley as the intersection is approached.

Since oblique faulting appears to be characteristic of a discontinuous stage of deformation in the wrench fault model, Searle and Laughton [1977] argue that the entire portion of small transforms between the adjacent rift valleys are probably kept in a state of 'initial shear' with the continual renewal of young sea-floor by intrusion and extrusion of magmas at the nearby junctions of the fracture zones with the spreading centers. If the wrench fault model is applicable near the junction of the Oceanographer transform with the median valley, because of the continual renewal of young sea-floor, then the oblique faulting observed in Figure 8 is not necessarily characteristic of a transform under compressional stresses.

Schroeder [1977] and Fox et al. [1978] observe northeast trending cusps in the bathymetry of the north wall of the Oceanographer transform that disrupt the continuity of the north wall. A detailed bathy-



metric survey (about 10 m contour interval) of the north wall of the transform recently conducted by French workers using a multi-narrow beam system (SEABEAM) confirms the existence of the large indentations on the north wall. Furthermore, the survey also delineates a series of smaller fractures on the north wall with similar trends as the cusps observed by Schroeder and Fox et al. [P. Fox and D. Needham, written communication, 1978].

Schroeder [1977] hypothesized that the large cusps on the north wall are related to offsets (left-lateral) of the central valley of the transform (I and II in Figure 6) and that they form a zone of fractures colinear with the trace of the offsets. The features identified by Schroeder are shown by the dashed lines in Figure 6 and 11. Schroeder and Fox et al. [1978] interpret these features as second-order faults that respond to stresses resulting from the adjusting transform. He suggests that most of the plate motion along the transform is accommodated by adjustment fractures parallel to the present-day direction of spreading [Menard and Atwater, 1968] near the ridge intersections and by motion along the N74°W trend near the center of the transform with some motion on the second-order faults. If the second-order faults are responding to the adjusting transform, it is reasonable to expect microearthquake activity along these features. We did not observe any microearthquake activity along the second-order faults delineated in Figures 6 and 11. Events of the same size as the events we located should be detected if they occurred along I and along the NE portion of II in Figure 6.

The trend of the located events in Figure 6 is similar to the trend of I and the microearthquakes appear to be a possible extension



of I. These are, however, not valid reasons for suggesting that the second-order features are seismically active since the trend of the zone of microearthquakes is sensitive to the velocity used to locate the events. A different velocity model could easily change the trend of the zone of microearthquakes from the trend of I. Thus, the hypothesis that the second-order features are responding to a transform under compression cannot be confirmed by the limited observations.

In summary, the focal-mechanism solution of a teleseismic earthquake and the inferred east-west direction of spreading suggest that the N74°W trending portion of the Oceanographer transform is under compressional stresses acting across its structural trends. The micro-earthquake observations near the eastern junction of the transform with the median valley are consistent with this suggestion but do not confirm it. Local observations of fault scarps and microearthquake activity near the central portion (N74°W trending section) of the transform could provide a test to confirm the hypothesis.

ACKNOWLEDGEMENTS

We are grateful to F. Schroeder for providing us with bathymetric charts he compiled prior to their publication and to P. Fox for a preprint. Thanks to D. Needham for information on preliminary observations of detailed bathymetry in our study area prior to their publication. We thank H. Kohler, and the officers and crew of the R/V VEMA for their valuable assistance. Special thanks go to W. McDonald, R. Bookbinder, G. Gunther and A. Hubbard for their work with the ocean-bottom seismographs. One of us, H. R., personally expresses his gratitude to K. McCamy for an introduction into ocean-bottom seismology. J. Ewing, P. W. Pomeroy, L. R. Sykes and A. Watts critically reviewed the manuscript. This study was supported under grants from the National Science Foundation, NSF DES74-24698 and NSF OCE76-82058 and the Office of Naval Research grant N00014-76-C-0818.

---

# REFERENCES

- Arcyana, Transform fault and rift valley from bathyscaph and diving saucer, Science, 190, 108-116, 1975.
- Courtillot, V., P. Tapponnier, and J. Varet, Surface features associated with transform faults: a comparison between observed examples and experimental model, Tectonophysics, 24, 317-329,
- Eittreim, S., and J. Ewing, Vema fracture zone transform fault, Geology, 3, 555-558, 1975.
- Fox, P.J., A. Lowrie, and B.C. Heezen, Oceanographer Fracture Zone, Deep-Sea Res., 16, 59-66, 1969.
- Fox, P.J., E. Schreiber, H. Rowlett, and K. McCamy, The geology of the Oceanographer Fracture Zone: a model for fracture zones, J. Geophys. Res., 81, 4117-4128, 1976.
- Fox, P.J., F.W. Schroeder, R.M. Moody, W.C. Pitman III, and P.J. Hoose, The bathymetry of the Oceanographer Fracture Zone and mid-Atlantic ridge at 35°N with implications for central North Atlantic plate motion, Deep Sea Res., in press, 1978.
- Francis, T.J.G., The ratio of compressional to shear velocity and rock porosity on the axis of the mid-Atlantic ridge, J. Geophys. Res., 81, 4361-4364, 1976
- Francis, T.J.G., and I.T. Porter, Median valley seismology: mid-Atlantic ridge near 45°N, Geophys. J. R. astr. Soc., 43, 279-311, 1973.
- Francis, T.J.G., I.T. Porter, and J.R. McGrath, Ocean-bottom seismograph observations on the mid-Atlantic ridge near lat. 37°N, Geol. Soc. Am. Bull., 88, 664-677, 1977.



- Helmberger, D.V., and G.B. Morris, A travel time and amplitude interpretation of a marine refraction profile: primary waves, J. Geophys. Res., 74, 483-494, 1969.
- Hill, D.P., A model for earthquake swarms, J. Geophys. Res., 82, 1347-1352, 1977.
- Isacks, B., L.R. Sykes, and J. Oliver, Focal mechanisms of deep and shallow earthquakes in the Tonga-Kermadec region and the tectonics of island arcs, Geol. Soc. Am. Bull., 80, 1443-1470, 1969.
- Kennett, B.L.N., and J.A. Orcutt, A comparison of travel time inversions for marine refraction profiles, J. Geophys. Res., 81, 4061-4070, 1976.
- Klein, F.W., P. Einarsson, and M. Wyss, The Reykjanes Peninsula, Iceland, earthquake swarm of September 1972 and its tectonic significance, J. Geophys. Res., 82, 865-888, 1977.
- Macdonald, K.C., Near-bottom magnetic anomalies, asymmetric spreading, oblique spreading, and tectonics of the mid-Atlantic ridge near lat. 37°N, Geol. Soc. Am. Bull., 88, 541-555, 1977.
- Macdonald, K.C., and B.P. Luyendyk, Deep-tow studies of the structure of the mid-Atlantic ridge crest near lat. 37°N, Geol. Soc. Am. Bull., 88, 621-636, 1977.
- McDonald, W.G., A.C. Hubbard, R.G. Bookbinder, and K. McCamy, Design and shipboard operation of a multipurpose ocean bottom seismograph, Mar. Geophys. Researches, 3, 179-196, 1977.
- Menard, H.W., and T.M. Atwater, Changes in direction of sea floor spreading, Nature, 219, 463-467, 1968.

- Mogi, K., Some discussion on aftershocks, foreshocks, and earthquake swarms — the fracture of a semi-infinite body caused by an inner stress origin and its relation to the earthquake phenomena, 3, Bull. Earthquake Res. Inst. Tokyo Univ., 615-658, 1963.
- Orcutt, J.A., B.L.N. Kennett, and L.M. Dorman, Structure of the East Pacific Rise from an ocean bottom seismometer survey, Geophys. J. R. astr. Soc., 45, 305-320, 1976.
- Pitman, W.C., P.J. Fox, P.J. Hoose, R.H. Moody, and E. Schreiber, The Oceanographer fracture zone revisited [abstract], EOS Trans. AGU, 55, 446, 1974.
- Prothero, W.A., I. Reid, M.S. Reichle, and J.N. Brune, Ocean bottom seismic measurements on the East Pacific Rise and Rivera Fracture Zone, Nature, 262, 121-124, 1976.
- Reid, I., The Rivera plate: a study in seismology and plate tectonics, Ph.D. Thesis, University of California, San Diego, Calif., 288 p., 1976.
- Reid, I., and K. Macdonald, Microearthquake study of the mid-Atlantic ridge near 37°N using sonobuoys, Nature, 246, 88-90, 1973.
- Schroeder, F.W., A geophysical investigation of the Oceanographer fracture zone and the mid-Atlantic ridge in the vicinity of 35°N, Ph.D. Thesis, Columbia University, New York, New York, 229 p., 1977.
- Searle, R.C., and A.S. Laughton, Sonar studies of the mid-Atlantic ridge and Kurchatov fracture zone, J. Geophys. Res., 82, 5313-5328, 1977.



- Shibata, T., and P.J. Fox, Fractionation of abyssal tholeiites: samples from the Oceanographer fracture zone (35°N, 35°W), Earth Planet. Sci. Lett., 27, 62-72, 1975.
- Spindel, R.C., S.B. Davis, K.C. Macdonald, R.P. Porter, and J.D. Phillips, Microearthquake survey of median valley of the mid-Atlantic ridge at 36°30'N, Nature, 248, 577-579, 1974.
- Sykes, L.R., Mechanism of earthquakes and nature of faulting on the mid-Atlantic ridge, J. Geophys. Res., 72, 2131-2153, 1967.
- Sykes, L.R., Earthquake swarms and sea-floor spreading, J. Geophys. Res., 75, 6598-6611, 1970.
- Talwani, M., C.C. Windisch, and M.G. Langseth, Reykjanes ridge crest: a detailed geophysical study, J. Geophys. Res., 76, 473-517, 1971.
- Tatham, R.H., and J.M. Savino, Faulting mechanisms for two oceanic earthquake swarms, J. Geophys. Res., 79, 2643-2654, 1974.
- Udias, A., A. Lopez Arroya, and J. Mezcuca, Seismotectonics of the Azores-Alboran region, Tectonophysics, 31, 259-289, 1976.
- Van Andel, T.H., R.P. Von Herzen, and J.D. Phillips, The Vema fracture zone and the tectonics of transverse shear zones in oceanic crustal plates, Mar. Geophys. Researches, 1, 261-283, 1971.
- Weidner, D.J., and K. Aki, Focal depth and mechanism of mid-ocean ridge earthquakes, J. Geophys. Res., 78, 1818-1831, 1973.
- Whitmarsh, R.B., Axial intrusion zone beneath the median valley of the mid-Atlantic ridge at 37°N detected by explosion seismology, Geophys. J. R. astr. Soc., 42, 189-215, 1975.
- Whitmarsh, R.B., Seismic refraction studies of the upper igneous crust in the North Atlantic and porosity estimates for layer 2, Earth Planet. Sci. Lett., 37, 451-464, 1978.

- Whitmarsh, R.B., and A.S. Laughton, A long-range sonar study of the mid-Atlantic ridge crest near 37°N (FAMOUS area) and its tectonic implications, Deep Sea Res., 23, 1005-1023, 1976.
- Wilcox, R.E. T.P. Harding, and D.R. Seely, Basic wrench tectonics, Am. Assoc. Petrol. Geol. Bull., 57, 74-96, 1973.
- Wilson, J.T., A new class of faults and their bearing on continental drift, Nature, 207, 343-347, 1965.



TABLE I — APPARENT VELOCITIES AND TIME INTERCEPTS

Profile	Second Arrivals		First Arrivals		dt/dh (sec/km)
	$V_2$ (km/sec)	$T_2$ (sec)	$V_3$ (km/sec)	$T_3$ (sec)	
West	3.03 <sup>†</sup>	2.61 <sup>†</sup>	5.93	3.11	0.45
East	----	----	5.29 <sup>†</sup>	3.03 <sup>†</sup>	0.45
North	----	----	6.50	3.39	0.60
South	----	----	4.35*	3.13*	0.65

\* Poorly determined

<sup>†</sup> Forced

FIGURE CAPTIONS

- Figure 1: Location map of study area on the mid-Atlantic ridge and the FAMOUS area. Hachured box is the area of the OBS experiment. Depth in meters, after Fox et al. [1978].
- Figure 2: Location of refraction experiment. Triangles are OBS locations. Thick lines represent the shooting tracks. Contour interval is in corrected meters. Bathymetry (meters) adapted from Schroeder [1977]. Depths less than 2000 m are denoted by open dots. Stipples denote depths greater than 3600 m.
- Figure 3: Plot of the cumulative number of events recorded by OBS 1 and OBS 3 near the intersection of the Oceanographer transform with the northern rift axis. The event rate is about 15 to 20 events per day. Note that OBS 3 detected a small swarm on day 337. On day 335 there is a sudden increase in the activity at OBS 3.
- Figure 4: Number of events as a function of time at OBS 3.
- Figure 5: Example seismograms of two microearthquakes recorded at OBS 1. The vertical, horizontal and hydrophone traces are denoted by V, HZ, and HP, respectively. Labeled phases are discussed in the text. The noise on the HP trace is a result of the playback electronics. a) Event at 1535 GMT on day 338 (not located). b) Event at 0205 GMT on day 337.



Figure 6: Basement contours of eastern part of Oceanographer transform fault adapted from Schroeder et al. [1977] along with OBS positions (triangles), satellite fixes used to locate OBS positions (squares), preferred (solid circles) and alternative (open circles) locations of microearthquake epicenters. Choices of epicentral locations are explained in text. Thick, dashed lines represent fault zones inferred by Schroeder et al. from offsets (I and II) in the transform valley (hachured area) and from changes in the basement contours on the walls of the transform fault. Depths to basement less than 200 m are stippled.

Figure 7: Seismograms of different earthquakes showing clear dilatational first motions (down) at arrow of P waves recorded by a hydrophone (HP) on OBS 1 and a vertical geophone (V) on OBS 3. The ranges of the earthquakes from OBS 3 and OBS 1 are 7.9 km and 16.2 km.

Figure 8: Physiographic provinces near the intersection of the northern rift valley with the eastern portion of the Oceanographer transform [adapted from Schroeder, 1977]. Note the change in the trends of major scarps. Closed circles are microearthquake epicenters located by the OBS array (triangles).

Figure 9: Focal-mechanism solution of earthquake of 17 May 1964 (event 1) on equal-area projection of the lower hemisphere of the focal sphere. North and east correspond

to top and right of projection, respectively. Closed and open symbols represent compressional and dilatational first motions, respectively. Squares denote data re-examined for this study. Circles are data determined by Sykes [1967]. Crosses indicate nodal arrivals. Only long-period data are used for the solution. Nodal planes determined by Sykes denoted by solid lines. Large, dashed line shows the major N74°W trend of the Oceanographer transform. Smaller symbols indicate unreliable data.

Figure 10: Focal-mechanism solution of earthquake of 17 April 1974 (event 3). Same projection of data and symbols as in Figure 9. Polarization of S wave is shown by line. Large circles indicate choice of first motions determined from long and short-period seismograms. Small circles indicate unreliable readings of first motions (some are short-period readings). Choice of polarity based only on long-period seismograms is indicated by squares. For comparison, the solution of the earthquake of 17 May 1964 by Sykes [1967] is denoted by short, dashed lines.

Figure 11: Basement contours of the Oceanographer transform (200 m contour interval). Interpretation of present trends, relic trends and 'second-order' faults for the fracture zone are by Schroeder [1977]. Small dots are microearthquake epicenters located by the OBS array. Focal-mechanism solutions of events 1 and 3. The solution of



event 3 (shown in Figure 10) is assumed to be the same as event 1 (shown in Figure 9). Locations of earthquakes by the International Seismological Centre (ISC).

Figure 12: Time-distance data from the refraction profiles recorded by OBS 1 and bathymetry beneath shooting track. Travel times (TT) are corrected for topography. Least-squares lines are calculated from travel-time data represented by closed circles. A prominent shadow zone occurs at ranges between 10 and 18 km along the west profile. a) West profile. b) South, north and east profiles.

Figure 13: Ray-traced residuals for first arrivals of the west profile. Travel-time differences between observed first arrivals of west profile (uncorrected for topography) and rays traced through three crustal models that include the topography beneath the west profile are plotted as a function of range. Vertical line at 3 km is standard error for reading first arrivals. Symbols denote average velocity used for the sea-bed layer in each model.

Figure 14: Reduced record section of refracted arrivals recorded from western line by the hydrophone of OBS 1 and bathymetry beneath shooting track. The reducing velocity is 6 km/sec. The amplitudes are not corrected for ranges or shot size and are compressed. The shot size is the same for distances greater than 8 km. The seismograms are digitized before the first arrival to the water-wave

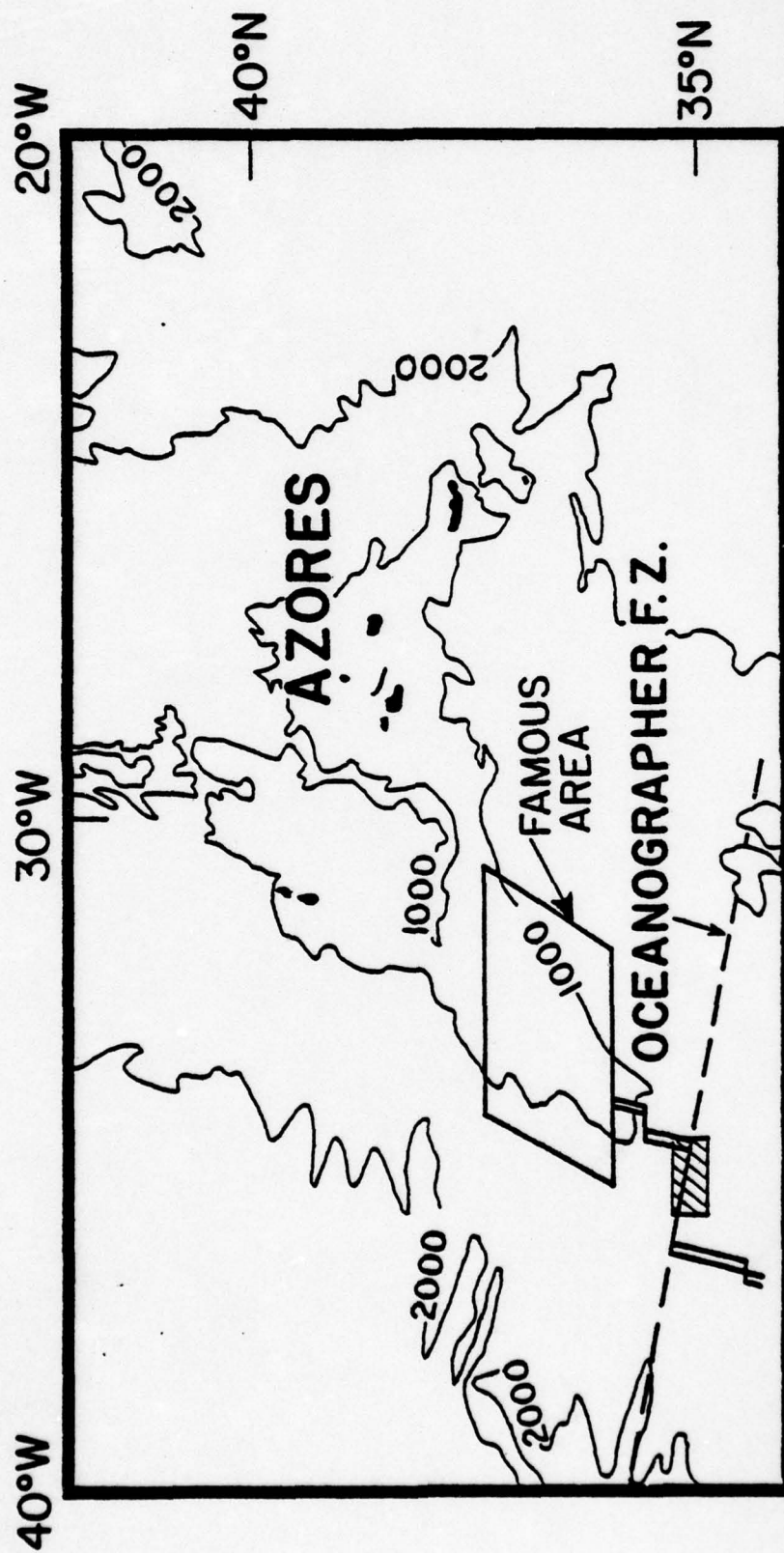


Figure 1

40



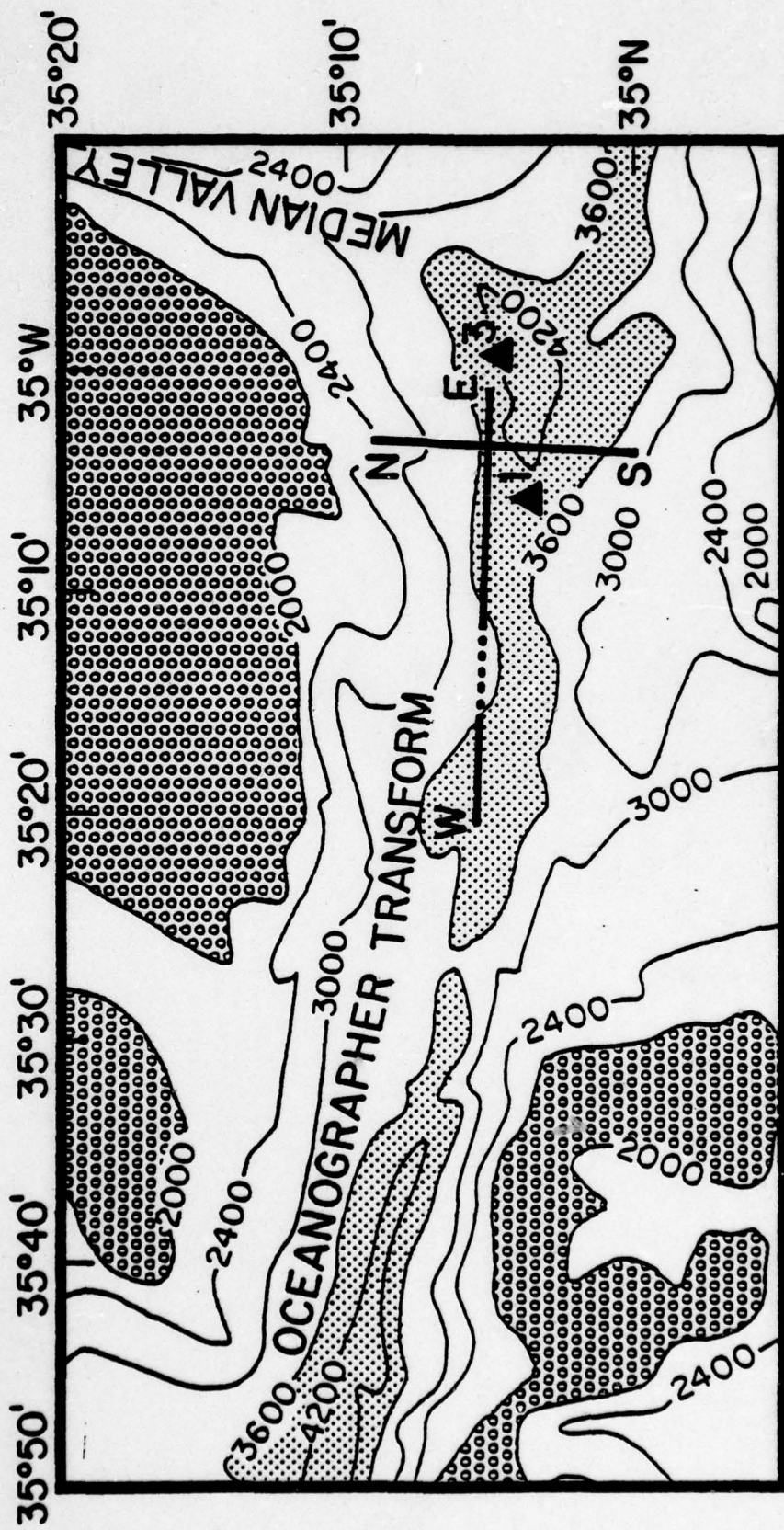


Figure 2

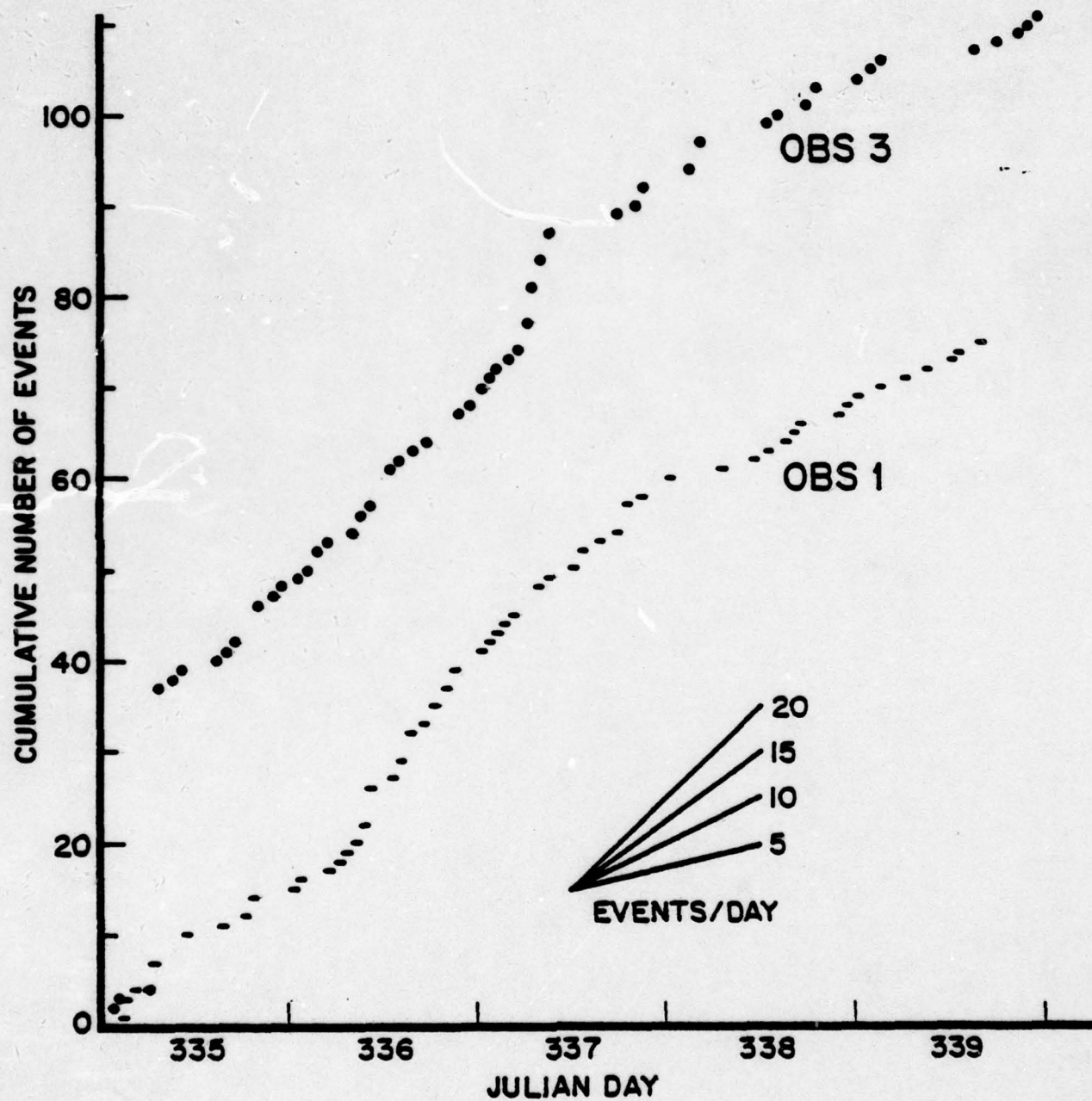


Figure 3



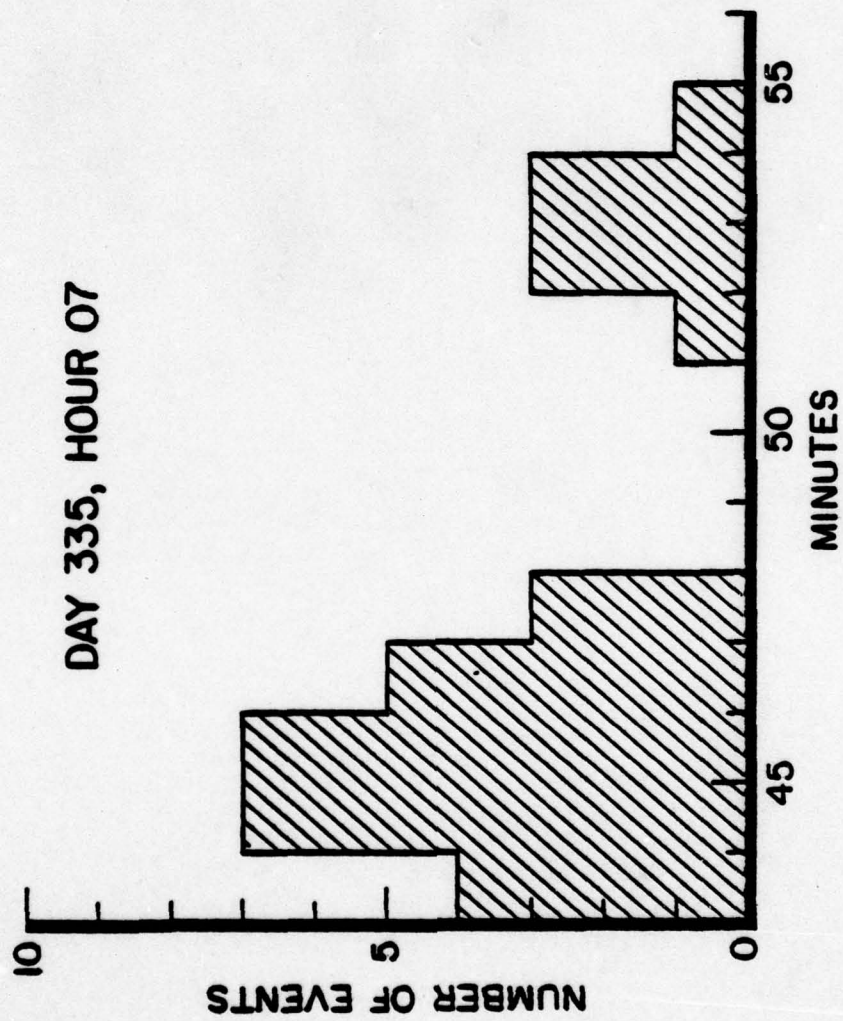


Figure 4

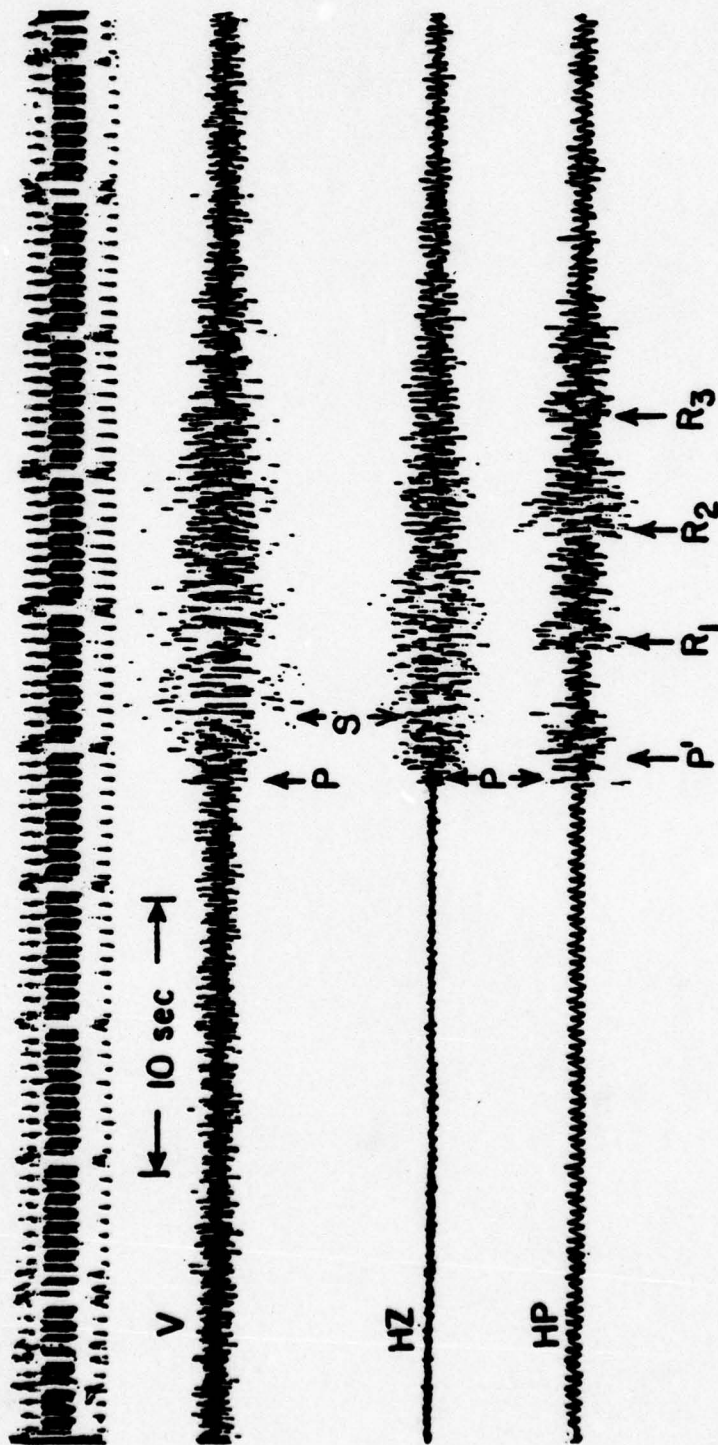


Figure 5a



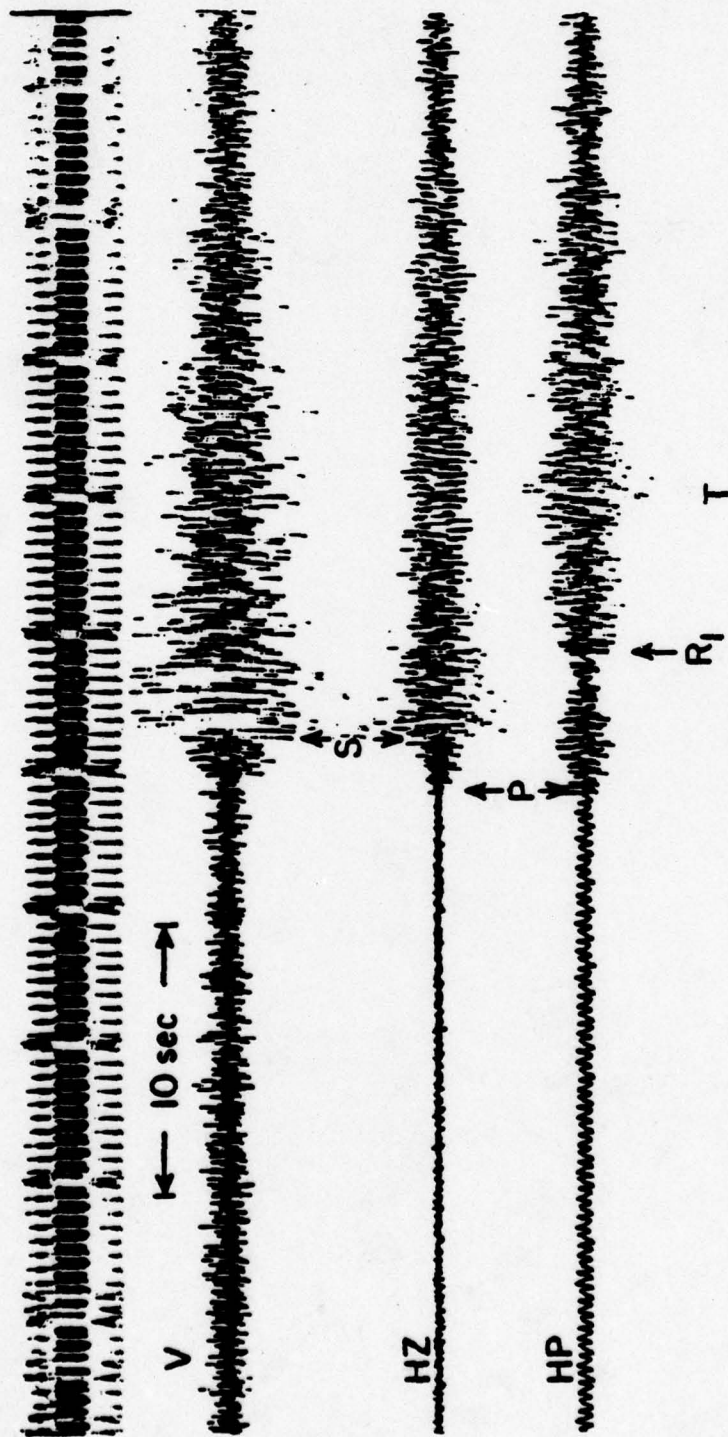


Figure 5b

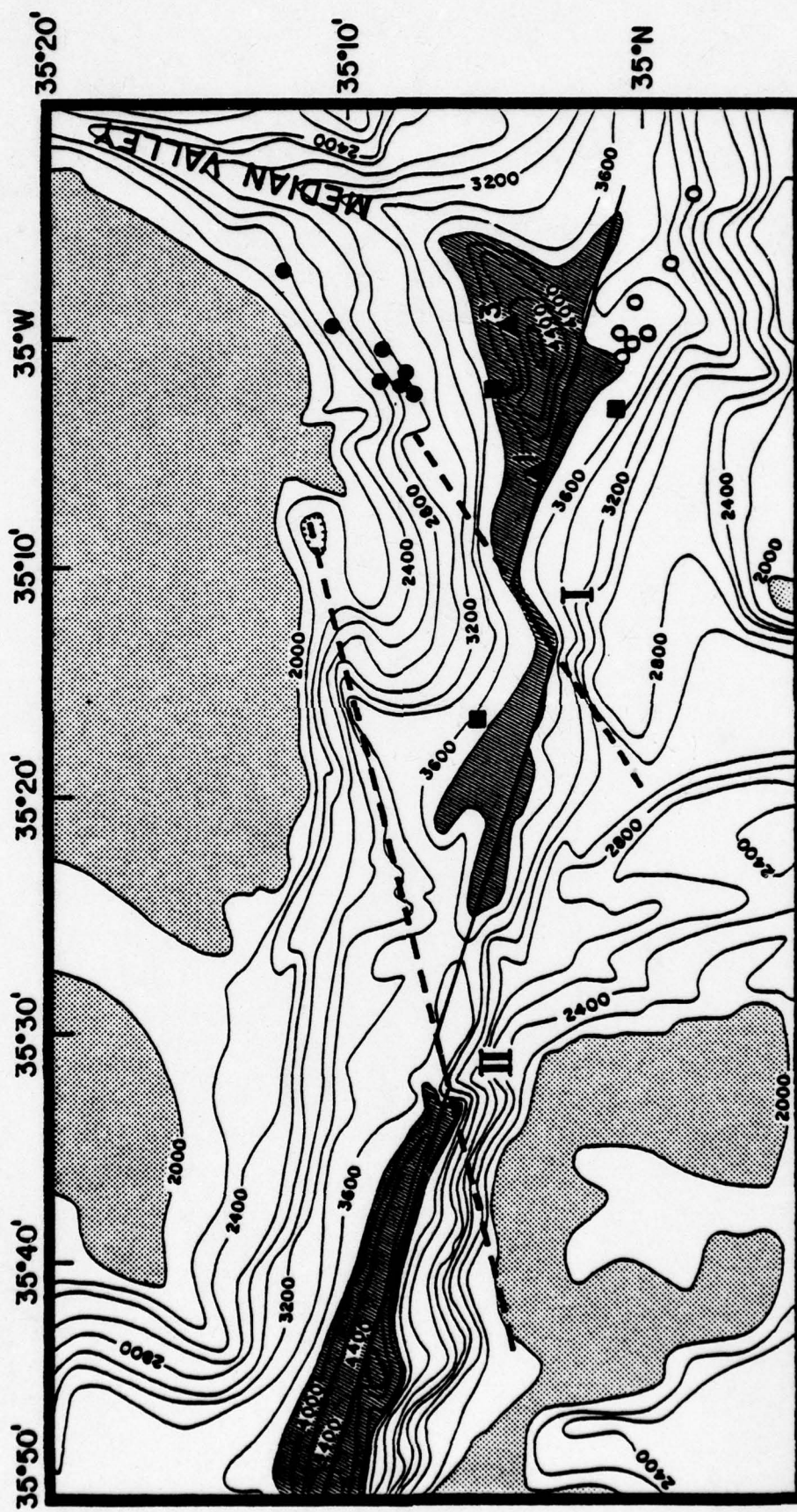
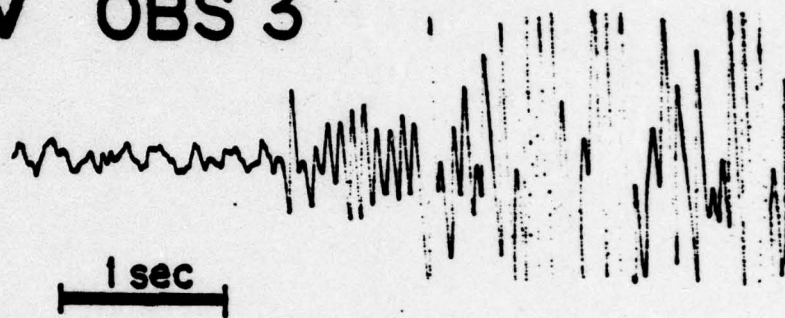


Figure 6



**V OBS 3**



**HP OBS 1**

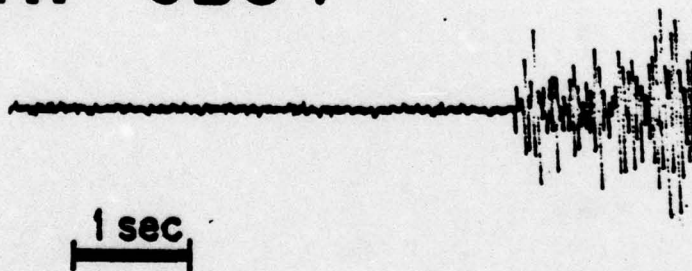


**Figure 7**



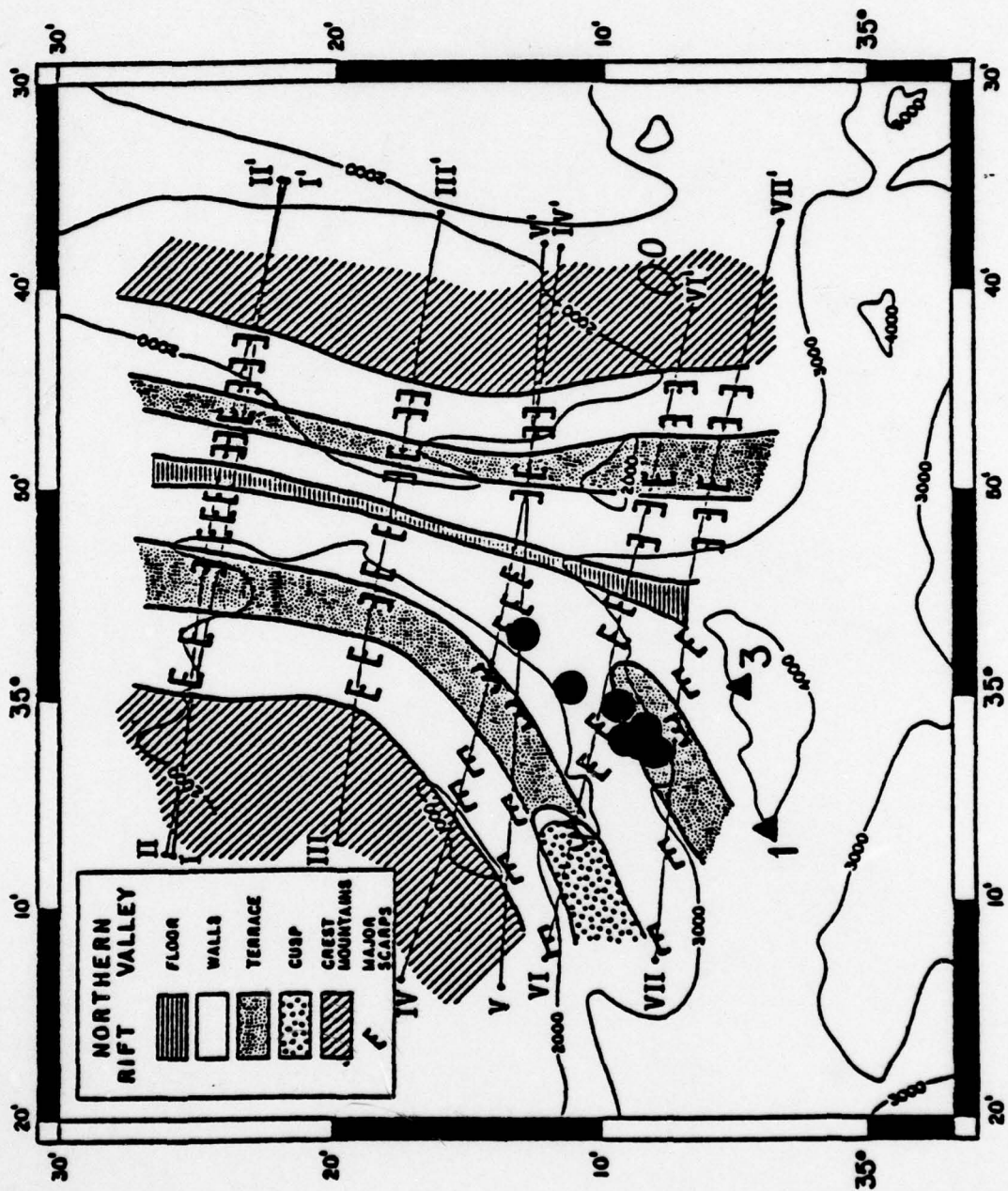
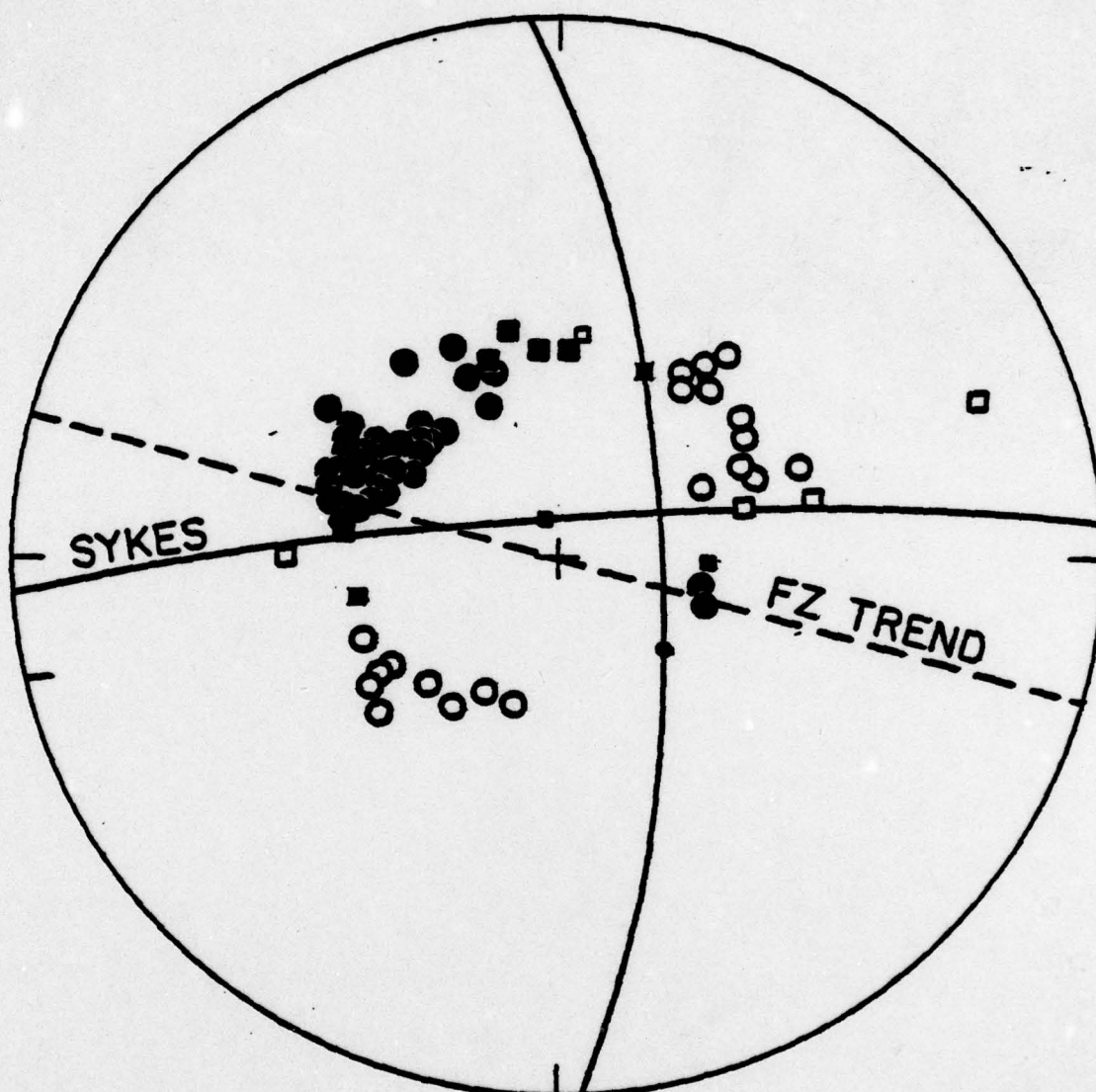


Figure 8



17 MAY 1964

Figure 9



**Figure 10**



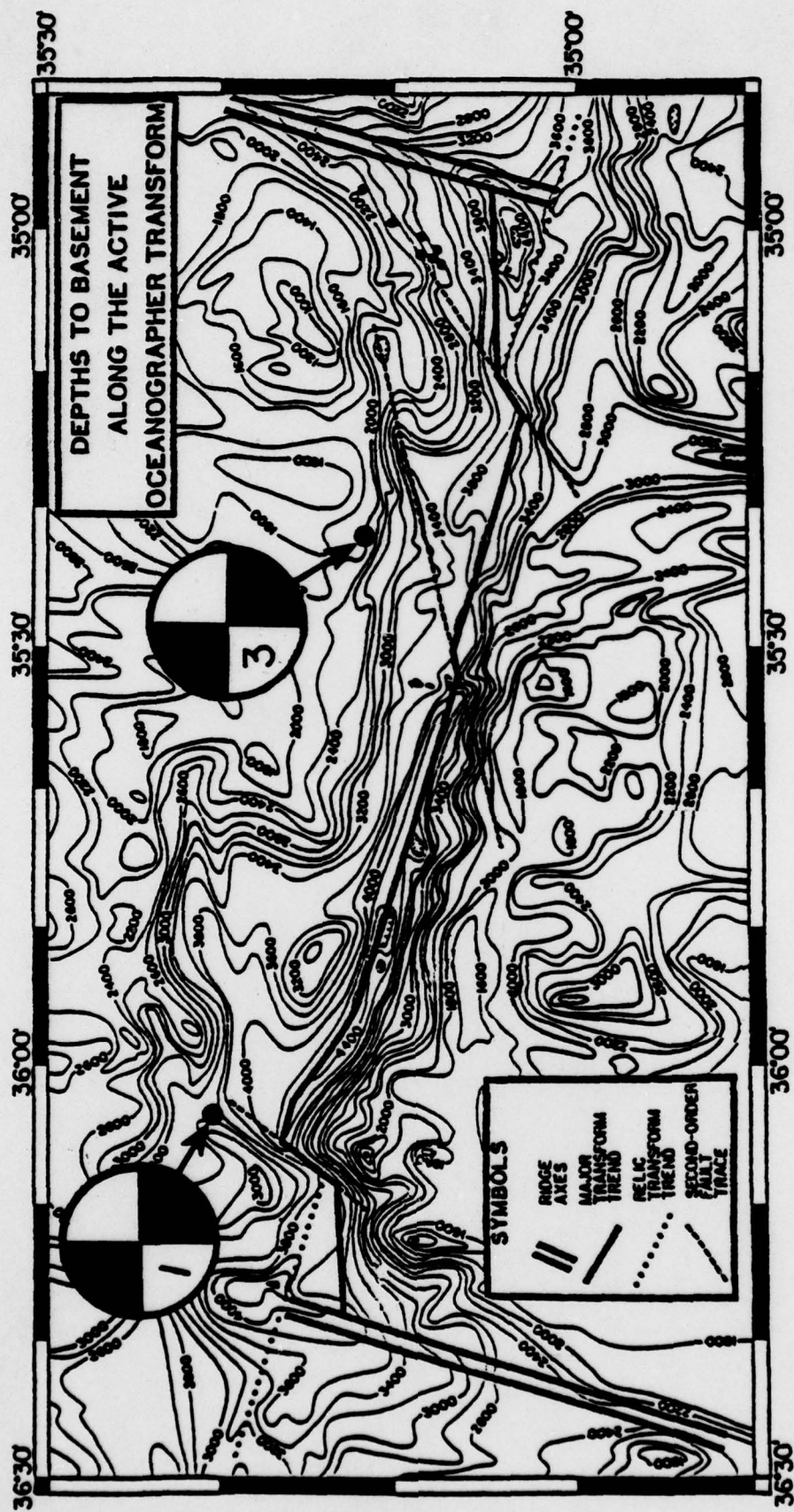


Figure 11

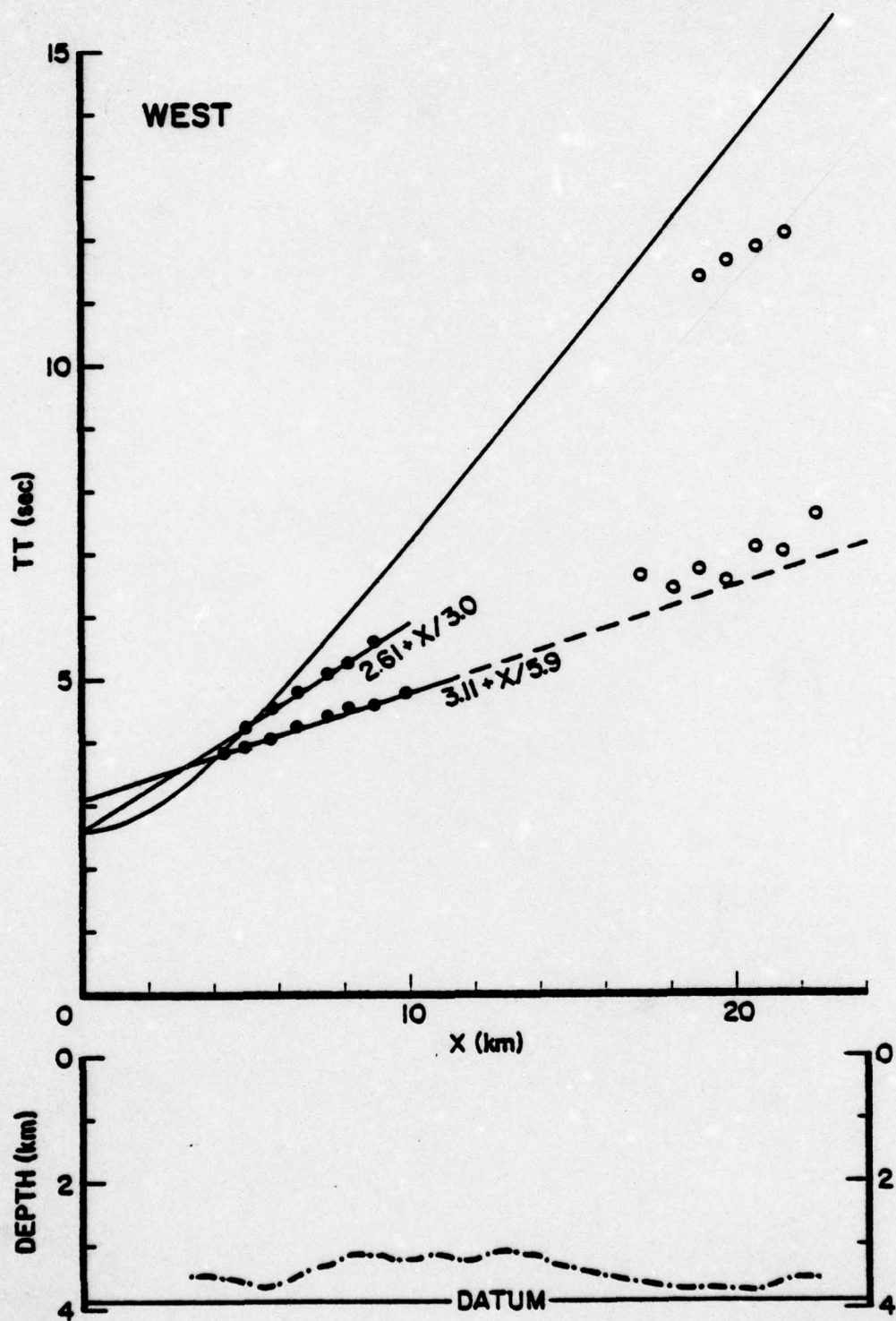


Figure 12a

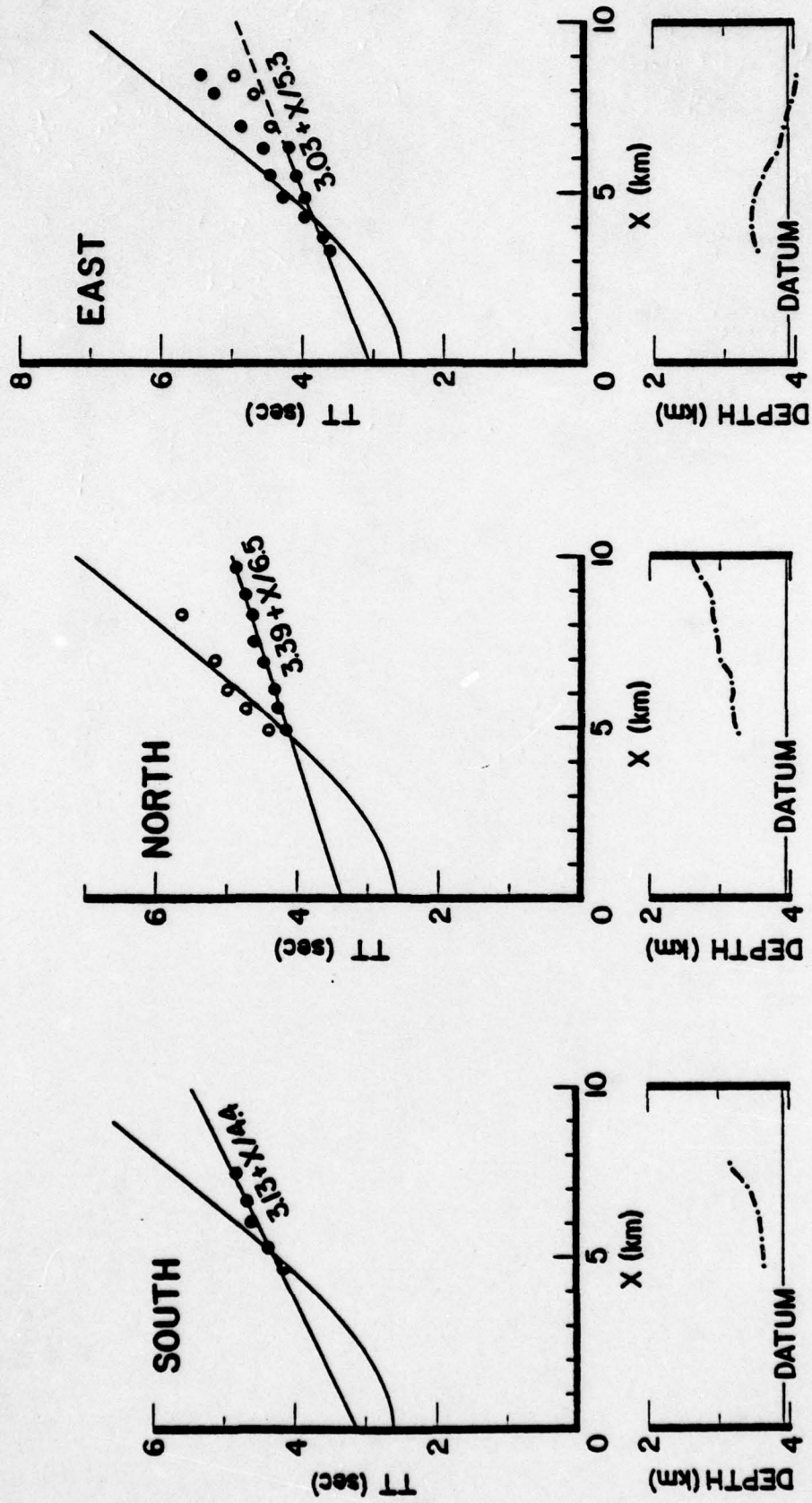


Figure 12b



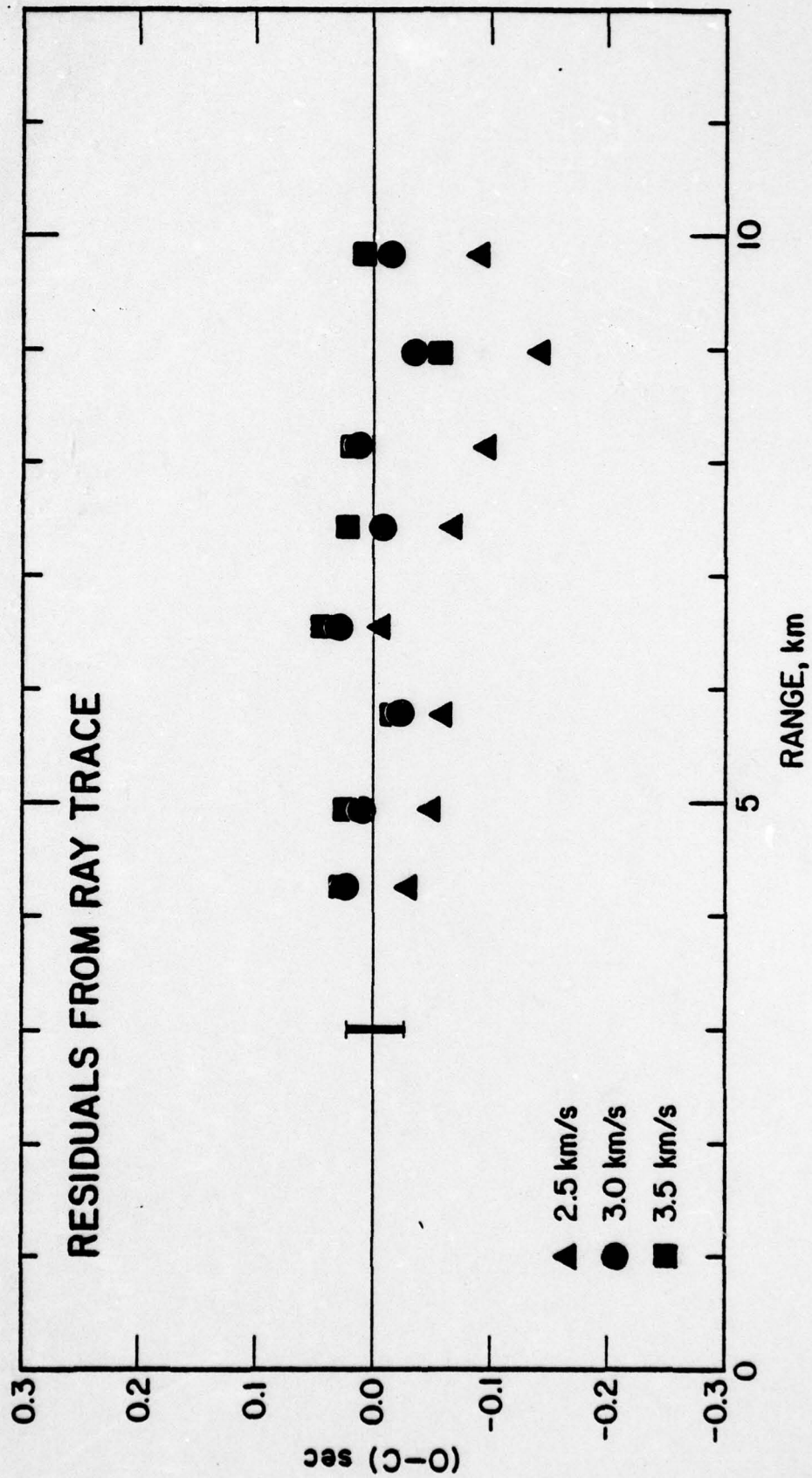


Figure 13

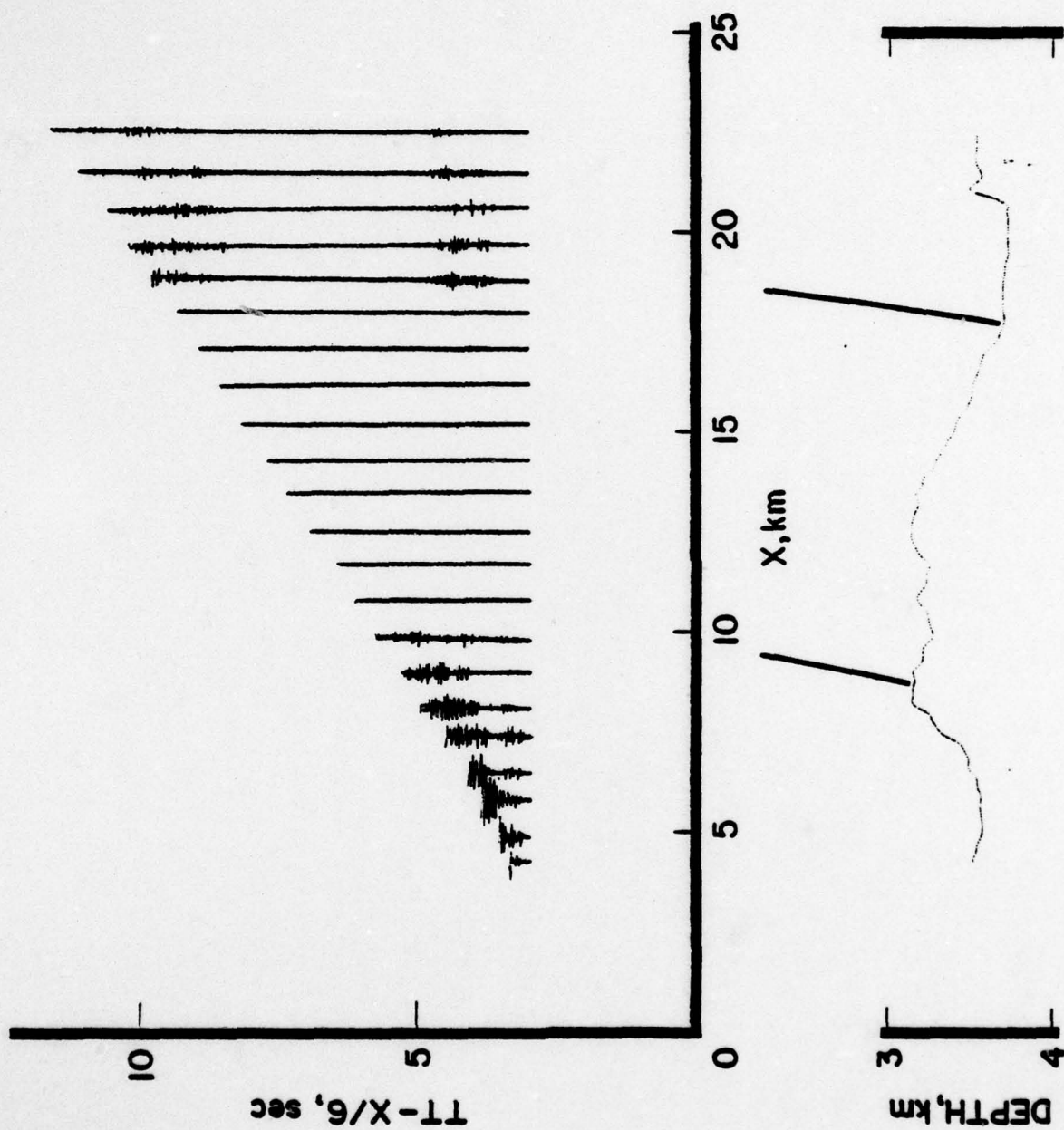


Figure 14

## APPENDIX

In this paper we use travel-time data alone to interpret the data. The instruments were not designed for the quantitative analysis of amplitudes [McDonald et al., 1977]. Furthermore, as shown for the west profile, the detailed velocity structure beneath the entire area of our experiment is probably too complex to be well constrained by our refraction data because of possible lateral changes in structure. Thus, existing methods for computing synthetic seismograms, since they assume lateral homogeneity, are of limited use here.

Kennett and Orcutt [1976] and Whitmarsh [1978] discussed the problems in marine refraction associated with the assumption of uniform layers or continuously varying velocity gradients as a velocity-depth model. Orcutt et al. [1976] and Helmberger and Morris [1969] presented models of the upper oceanic crust, using both amplitude and travel time analysis, that suggest that strong velocity gradients exist in the upper oceanic crust. We do not have the information to discriminate between these models here and, for simplicity, assume a velocity-depth model with uniform layers that can be compared with other work in the literature.

### Seismograms and Time-Distance Plots

Seismograms of OBS 1 commonly exhibit two ground wave arrivals prior to the arrival of the direct water wave. First arrivals, though detected by all the components, have the best signal-to-noise ratios on the hydrophone channel. Consequently, all travel time measurements



are made on that channel. The standard errors in picking first arrivals, average about 0.03 sec on all the profiles for ranges less than 10 km. Corrections to the origin times of the shots, the static corrections, have errors that rarely exceed 0.02 sec and are usually much less.

Second arrivals commonly have large amplitudes on the horizontal and the hydrophone channels. The amplitudes of the second arrivals are generally larger than those of the first arrivals. The large amplitudes of the second arrivals on the horizontal channels compared to those arrivals on the vertical channels suggest that the second arrival propagates as a compressional wave at shallower depths below the sea-floor than the first arrivals. The large amplitudes of the second arrivals also suggest that these waves are propagating through crust with a velocity gradient [Kennett and Orcutt, 1976]. The standard error in picking the second arrival is at least 0.05 sec and usually is much larger. Interference with phases that correspond to the bubble-pulse oscillation of the first arrival is partially responsible for the larger error in picking the second arrival.

We correct the travel times for the bottom relief along the seismic profiles using the method discussed by Whitmarsh [1975]. This method retains the water layer and flattens the sea-bed to a horizontal datum, here, the water depth of the OBS. This kind of topographic correction is sensitive to the velocity of the material causing the bottom relief. We varied the velocity of the sea-floor until we found the value of the correction coefficient,  $dt/dh$ , that minimized the root-mean-square (RMS) of the travel time residuals for each group of arrivals that we interpret to have the same apparent

velocity. This method assumes that the refracting horizons approximate planes. Another method, used by Kennett and Orcutt [1976], removes the water layer and assumes that velocity surfaces parallel the sea-floor. Each of the above methods represent different assumptions about the velocity structure of the earth. The method of Whitmarsh, however, has the same effect on apparent velocities as that used by Kennett and Orcutt when the value of  $dt/dh$  approaches its maximum for a given refractor. That is, when the variation in travel times is a function of the velocity contrast of the water and the refractor.

Time-distance data for OBS 1, corrected for topography, in Figure 12 show the apparent velocities computed from some of the time-distance data are probably meaningless. There is considerable scatter in the first arrivals and second arrivals of the east line and the second arrivals of the north line. The effect of the topographic corrections on the travel-time residuals for the above mentioned data is consistent with this conclusion. For the various topographic corrections applied to the first and second arrivals of the east line ( $0.02 \leq dt/dh \leq 0.65$ ) the scatter of the arrival-time residuals actually increased. Topographic corrections applied to second arrivals of the west line do not produce a minimum in the travel-time residuals. The south line has too few arrivals for the short interval of ranges along this profile for there to be any confidence in correctly interpreting apparent velocities from the data of this line.

It is possible to compute apparent velocities that we can interpret in terms of a layered model for first arrivals of the north profile and west profile (arrivals from shots less than 10 km). For



the travel-time data of these two profiles there is a value of  $dt/dh$  that gives a distinct minimum in the travel time residuals. These data show the importance of applying the proper travel time corrections to calculate apparent velocities in areas with rough topography. For example, apparent velocities calculated for first arrivals from the west profile vary from 5.4 km/sec to 6.7 km/sec for correction coefficients between 0.65 sec/km and 0.2 sec/km. The correct  $dt/dh$  yields an apparent velocity of 5.9 km/sec. The time intercepts, however, are less sensitive to the value of  $dt/dh$ . Apparent velocities corresponding to the minimum RMS of the travel-time residuals of first arrivals for the north and west lines are listed in Table I.

#### Crustal Model of the Transform Valley

It is difficult to estimate the actual velocity of the material that lies above the main refracting horizon (main refractor) in the central valley of the transform since there is some uncertainty in calculating the apparent velocity and time intercept for second arrivals of the west profile. For the purpose of solving for the actual velocity of the main refractor we use as an initial guess the apparent velocity of the second arrivals calculated from the same  $dt/dh$  (0.45 sec/km) used to calculate the apparent velocities of the first arrivals along the west profile, since solving for the actual velocity of the main refractor is quite insensitive to our choice for the average velocity of the upper layer.

To estimate the velocity of the main refractor in the central valley we assume that the apparent velocities are controlled, to a



first approximation, by dip. Travel times from first arrivals on the east profile are combined with the west profile to form a split profile. Again, we chose to use apparent velocities for first arrivals on the east profile (arrivals with ranges less than 6.5 km and not severely affected by the rough relief along this profile) calculated from  $dt/dh$  equal to 0.45 sec/km. This topographic correction gives an intercept time that satisfies the assumption of a split profile within the errors of the intercept times implying that we have some control on the velocity of the main refractor. The actual velocity determined this way is 5.6 km/sec.

The depth and dip of the main refractor beneath OBS 1 is more dependent upon the average velocity of the material above it than the velocity is. Consequently, we solve for the depth and dip of the main refractor several times using velocities of 2.5, 3.0 and 3.5 km/sec for the layer above the main refractor. We trace rays through several crustal models that include the topography of the sea-floor beneath the west profile and the depths and dips of the main refractor that we calculate earlier. Total travel times of the traced rays for each model are subtracted from observed travel times, uncorrected for topography, to compute residuals for the models.

Travel-time residuals for each model are plotted in Figure 13. A model with an average velocity of 3.0 km/sec for the layer gives residuals that are within the standard error (vertical line in Figure 13) of travel-time picks. Thus, a crustal model beneath OBS 1 that satisfies the observed travel times consists of a 3.0 km/sec layer, 1 km thick, over a 5.6 km/sec refractor dipping  $2^\circ$  towards the east.